
Revealing Multimodal Contrastive Representation Learning through Latent Partial Causal Models

Yuhang Liu¹ Zhen Zhang¹ Dong Gong² Biwei Huang³ Mingming Gong⁴ Anton van den Hengel¹
Kun Zhang⁵ Javen Qinfeng Shi¹

Abstract

Multimodal contrastive representation learning methods have proven successful across a range of domains, partly due to their ability to generate meaningful shared representations of complex phenomena. To enhance the depth of analysis and understanding of these acquired representations, we introduce a unified causal model specifically designed for multimodal data. By examining this model, we show that multimodal contrastive representation learning excels at identifying latent coupled variables within the proposed unified model, up to linear or permutation transformations resulting from different assumptions. Our findings illuminate the potential of pre-trained multimodal models, *e.g.*, CLIP, in learning disentangled representations through a surprisingly simple yet highly effective tool: linear independent component analysis. Experiments demonstrate the robustness of our findings, even when the assumptions are violated, and validate the effectiveness of the proposed method in learning disentangled representations.

1. Introduction

As humans, we often encounter situations where being aware of a signal from one modality helps in the interpretation of another. For instance, observing someone’s facial expressions while they speak facilitates comprehension beyond merely listening to the audio. Similarly, in machine learning, there are often instances where data from one modality can enhance the interpretation of another. This

becomes particularly valuable in situations where obtaining explicit training labels is challenging or resource-intensive (Quattoni et al., 2007; Shi et al., 2019). One promising strategy in this context is to use data from one modality, *e.g.*, text data, as a supervision signal in the interpretation of another, *e.g.*, image data (Mori et al., 1999; Wang et al., 2009; Ramanathan et al., 2013; He & Peng, 2017; Radford et al., 2021). The primary approach for achieving this is known as *multimodal contrastive representation learning*, which focuses on optimizing a symmetric contrastive loss (Zhang et al., 2022; Radford et al., 2021), *e.g.*, a symmetric adaptation of the standard contrastive loss (Wu et al., 2018; Tian et al., 2020; He et al., 2020; Chen et al., 2020). The learned representations, guided by the symmetric contrastive loss, have been applied in a variety of applications, including zero/few-shot learning (Radford et al., 2021; Zhou et al., 2022a), domain generalization (Zhou et al., 2022a;b), and robustness to adversarial examples (Ban & Dong, 2022). Despite its proven success in practice, understanding the effectiveness of learned representations presents a non-trivial challenge.

Previous studies investigated the effectiveness of standard contrastive learning (on a single modality) by exploring the connection between the learned representations and the latent variables in latent causal generative models (Zimmermann et al., 2021; Von Kügelgen et al., 2021). This exploration offers a vital causal viewpoint, highlighting the use of independent causal mechanisms (Schölkopf et al., 2021; Rojas-Carulla et al., 2018) to understand the generalization ability of these learned representations across various downstream applications. However, these studies are predominantly restricted to single-modality scenarios, typically images. The nature of the relationship between the representations learned by the symmetric contrastive learning in multimodal settings and the latent variables within latent causal generative models remains under-explored. Further related works are detailed in Appendix A.1.

The existence of the close connection between the representations learned in multimodal contrastive learning and the latent variables in latent causal generative models can be revealed from the symmetric contrastive loss and recovering the latent variables. Specifically, the goals of multimodal

¹Australian Institute for Machine Learning, The University of Adelaide, Australia ²School of Computer Science and Engineering, The University of New South Wales, Australia ³Halicioğlu Data Science Institute (HDSI), University of California San Diego, USA ⁴School of Mathematics and Statistics, The University of Melbourne, Australia ⁵Department of Philosophy, Carnegie Mellon University, USA. Correspondence to: Yuhang Liu <yuhang.liu01@adelaide.edu.au>.

contrastive learning, *i.e.*, aligning real pairs and separating incorrect ones (Zhang et al., 2022; Radford et al., 2021), mirror the essential objectives in solving inverse problems. In this perspective, aligning real pairs in multimodal contrastive learning is closely related to matching a type of prior information on latent variables while separating the incorrect pairings, aiming for capturing the full range and complexity of the latent variables. Accordingly, we demonstrate the connection between the two paradigms formally in the following.

We introduce a novel latent partial causal model to formulate multimodal contrastive learning, with the reflection of their natural connection. It formulates the causal generative process of the paired observations and the latent variables capturing the modality-specific and shared patterns. Specifically, we propose to capture the cross-modality *shared* patterns relying on a coupling relation between a couple of *separate* latent variables. Unlike previous works employing a *single* latent variable to model the shared patterns (Daunhawer et al., 2023; Gresele et al., 2020; Yao et al., 2023), the proposed method uses *coupling* relation and *separate* latent variables (*i.e.*, *latent coupled variables*) to capture the flexible cross-modality matching relationship in practical multimodal contrastive learning (*e.g.*, CLIP) more generally. Apart from the flexibility and generalization, furthermore, benefiting from the modeling with separate and coupled latent variables, we show that *all* latent coupled variables in the proposed causal model can be identified *up to linear or permutation transformations*, subject to specific statistical assumptions. This finding sets our work apart from prior studies focused on *partial and block* identifiability (Daunhawer et al., 2023; Yao et al., 2023), *e.g.*, identifying part of latent coupled variables up to an invertible nonlinear mapping, thus offering a more comprehensive and fine-grained understanding for representations learned by multimodal contrastive representation learning.

The theoretical insights above reveal a remarkable facet of multimodal contrastive learning, showcasing their inherent and potent capacity to learn disentangled representations, under specific conditions. This remarkable ability can be brought to light for multimodal contrastive learning and the pre-trained models, such as CLIP (Radford et al., 2021), through the application of a straightforward yet highly effective tool, linear independent component analysis (ICA) (Hyvärinen et al., 2001). This provides the first step towards a guarantee for the disentanglement ability of multimodal contrastive representation learning. We validate our theoretical findings under ideal assumptions, and illustrate the robustness of our findings even when the assumptions are partially violated. We conduct experiments on real datasets, demonstrating the disentanglement ability of pre-trained CLIP when combined with the Fast ICA method (Hyvärinen, 1999), in terms of learning disentangled representa-

tions, few-shot learning and domain generalization.

2. Motivation and The Proposed Model

In this section, we begin by providing a basic motivation for the connection between representations learned by multimodal contrastive representation learning and the latent variables in latent causal generative models in Section 2.1. Building upon this motivation, we then introduce a novel latent partial causal model and clarify how this model differs from previous works, specifically those by (Zimmermann et al., 2021; Von Kügelgen et al., 2021; Daunhawer et al., 2023; Gresele et al., 2020; Yao et al., 2023), in Section 2.2.

2.1. Motivation: Relation with Inverse Problem

Multimodal contrastive representation learning leverages latent shared patterns in multimodal data, by utilizing information from one modality to supervise another. Recent developments in this field show that representations learned through a symmetric contrastive loss are effective in various downstream tasks, such as transfer learning, and are robust to shifts in natural distributions (Radford et al., 2021). The contrastive loss function is designed to maximize the similarity in the embedding space between modalities for real pairs, while minimizing the similarity for incorrect pairs. Formally, the optimization objective is as follows:

$$\begin{aligned} \mathcal{L} = & -\frac{1}{N} \sum_{i=1}^N \log \frac{e^{d(\mathbf{f}_x(\mathbf{x}_i), \mathbf{f}_t(\mathbf{t}_i)) / \tau}}{\sum_{j=1}^N e^{d(\mathbf{f}_x(\mathbf{x}_i), \mathbf{f}_t(\mathbf{t}_j)) / \tau}} \\ & -\frac{1}{N} \sum_{i=1}^N \log \frac{e^{d(\mathbf{f}_x(\mathbf{x}_i), \mathbf{f}_t(\mathbf{t}_i)) / \tau}}{\sum_{j=1}^N e^{d(\mathbf{f}_x(\mathbf{x}_j), \mathbf{f}_t(\mathbf{t}_i)) / \tau}}, \end{aligned} \quad (1)$$

where d denotes a distance metric, *e.g.*, cosine similarity on hypersphere or L1 norm on convex bodies, τ is a learnable temperature parameter, N denotes the sample size, which means that we have N positive pairs and $N^2 - N$ negative pairs, \mathbf{f}_x denote the encoder on one modality \mathbf{x} , *e.g.*, image, similarly, \mathbf{f}_t denote the encoder on another \mathbf{t} , *e.g.*, text.

To further understand the symmetric contrastive loss, we investigate its asymptotics as follows:

Theorem 2.1 (Asymptotics of \mathcal{L}). *For fixed $\tau > 0$, as the sample size $N \rightarrow \infty$, the (normalized) symmetric contrastive loss converges to*

$$\begin{aligned} \lim_{N \rightarrow \infty} \mathcal{L} - 2 \log N = & -2 \mathbb{E}_{(\mathbf{x}, \mathbf{t}) \sim p(\mathbf{x}, \mathbf{t})} [d(\mathbf{f}_x(\mathbf{x}), \mathbf{f}_t(\mathbf{t})) / \tau] \\ & + \mathbb{E}_{\mathbf{x} \sim p(\mathbf{x})} \left[\log \mathbb{E}_{\mathbf{t} \sim p(\mathbf{t})} [e^{d(\mathbf{f}_x(\mathbf{x}), \mathbf{f}_t(\mathbf{t})) / \tau}] \right] \\ & + \mathbb{E}_{\mathbf{t} \sim p(\mathbf{t})} \left[\log \mathbb{E}_{\mathbf{x} \sim p(\mathbf{x})} [e^{d(\mathbf{f}_x(\mathbf{x}), \mathbf{f}_t(\mathbf{t})) / \tau}] \right]. \end{aligned} \quad (2)$$

Proof sketch The proof can be accomplished by adapting the proof methodology utilized in Theorem 1 of Wang & Isola (2020) for a single modality to the context of multiple modalities. It primarily relies on the application of the strong law of large numbers and the continuous mapping theorem. Refer to Appendix A.2 for details.

Insight Our primary insight is that the loss function Eq. (2) is intricately linked to two fundamental elements crucial for solving inverse problems, *e.g.*, with nonlinear ICA: 1) *Matching prior information on latent variables, i.e.*, the solution space is constrained by prior distribution, helping to mitigate issues of non-uniqueness in inverse problems. 2) *Recovering all information in latent space, e.g.*, ensuring that the inverse problem solution captures the full range and complexity of the latent variables.

Relation with Matching Prior Information To clarify this point, let us focus on the first term at the right-hand side of Eq. (2). In a multi-model setting, one modality plays a crucial role as a supervised signal for another modality. This implies that one modality can serve as potential prior knowledge. Let us consider the modality of text as this prior knowledge. By minimizing the first term, which reduces the distance between features obtained by encoders for real pairs, we essentially ensure the features generated by one encoder, *e.g.*, on the image modality, closely approximate the prior knowledge provided by the text. This closely aligns with a key element essential for solving inverse problems: matching prior information. For instance, when recovering latent variables from observational data, we expect the recovered variables to closely approximate the prior knowledge derived from the true latent variables.

Relation with Recovering All Information To elucidate this point, let us focus on the last two terms on the right-hand side of Eq. (2). Essentially, these two terms are approximately equal to optimizing the following (Proof can be found in Appendix A.3):

$$-H(p(\mathbf{f}_x(\mathbf{x})), p(\mathbf{f}_t(\mathbf{t}))) - H(p(\mathbf{f}_t(\mathbf{t})), p(\mathbf{f}_x(\mathbf{x}))), \quad (3)$$

Here, $H(\cdot, \cdot)$ represents the cross entropy. When both \mathbf{f}_x and \mathbf{f}_t transform \mathbf{x} and \mathbf{t} into uniformly distributed random variables, respectively, Equation (3) reaches its optimal solution. This uniform distribution underscores our goal of finding functions \mathbf{f}_x and \mathbf{f}_t that maximize information preservation. This objective aligns with a crucial aspect of solving inverse problems, which is to recover all latent space information.

Expanding upon the insight presented, we posit that multimodal contrastive representation learning has the potential to identify certain latent variables. The pertinent question is what latent variables in a latent causal generative model are

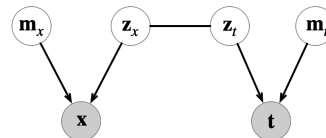


Figure 1. Illustration of the proposed latent partial causal model: The latent space is partitioned into $(\mathbf{m}_x, \mathbf{z}_x)$ and $(\mathbf{m}_t, \mathbf{z}_t)$, where \mathbf{m}_x and \mathbf{m}_t represent modality-specific latent variables. An undirected edge between \mathbf{z}_x and \mathbf{z}_t is employed to model latent shared patterns. The observations \mathbf{x} (*e.g.*, images) and \mathbf{t} (*e.g.*, text) are generated by two distinct generative processes, $\mathbf{g}_x(\mathbf{m}_x, \mathbf{z}_x)$ and $\mathbf{g}_t(\mathbf{m}_t, \mathbf{z}_t)$, respectively.

identified. Subsequent sections will introduce a novel latent causal generative model to elucidate this connection.

2.2. The Proposed Latent Partial Causal Model

Figure 1 illustrates the proposed latent partial causal model. In this model, the whole latent space is partitioned into two parts, each representing a different modality, *e.g.*, image and text. More specifically, to model latent shared patterns, an undirected edge is established between \mathbf{z}_x and \mathbf{z}_t to allow subtle perturbation, which will be formulated by conditional distributions in the next section. The rationale behind this modeling approach is grounded in the recognition that real-world multimodal data is often complex, noisy, and multifaceted. On one hand, the assertion ‘a picture is worth a thousand words’ is well-supported in literature (Groppe, 1963; Hum et al., 2011), emphasizing the rich detail and information that images can convey compared to text. Conversely, this notion is not universally applicable as argued by Reinert (1976), who suggests that sometimes textual information can be more informative than visual data. This perspective is further echoed by Fidler et al. (2013) in their assertion that ‘a sentence is worth a thousand pixels,’ highlighting the potential of text in conveying complex ideas succinctly.

In addition, we introduce \mathbf{m}_x and \mathbf{m}_t modality-specific latent variables, each tailored to capture the unique characteristics of their respective domains. For example, \mathbf{m}_x could encode information focusing on aspects like the presence of background noise or other visual artifacts that contribute to the overall composition of an image. On the other hand, \mathbf{m}_t could encode information about sentence structure or linguistic patterns that are characteristic of the grammar in textual content. Finally, the observations are associated with two distinct generative processes. Specifically, \mathbf{x} (*e.g.*, images) are generated through the process $\mathbf{g}_x(\mathbf{m}_x, \mathbf{z}_x)$, while observation \mathbf{t} (*e.g.*, text) come into existence through the generative process $\mathbf{g}_t(\mathbf{m}_t, \mathbf{z}_t)$.

Differences with previous works The proposed model distinguishes itself from previous works such as (Zimmer-

mann et al., 2021; Von Kügelgen et al., 2021), which leverage latent causal models to elucidate contrastive learning. Prior efforts predominantly concentrate on single-modal settings, while our proposed model extends this perspective to the more intricate domain of multi-modal settings. Loosely speaking, the proposed model can be considered a generalization of previous works. This generalization is apparent as the proposed model seamlessly reduces to a single-modal setting when the mixing functions from latent space to observed space are enforced to be identical, and specific variables are omitted. Furthermore, our model differs from previous works specifically designed for multi-modal settings (Daunhawer et al., 2023; Gresele et al., 2020; Yao et al., 2023), a distinction that becomes evident across two key dimensions: 1) Modeling shared patterns: the proposed model captures shared patterns across modalities allowing for the existence of a coupling relation in multimodal data. In contrast, previous works often achieve this by introducing the same variables. Notably, our modeling approach using the coupling relation is more general, as it can be reduced to using the same variables by enforcing an identical mapping on the coupling relation. 2) Identifiability results: The identifiability results obtained from the proposed model diverge from those found in previous works (Daunhawer et al., 2023; Yao et al., 2023), both in terms of breadth and depth of identifiability, due to the introduction of the coupling relation (will be demonstrated in Section 3). a) (Breadth of Identifiability) Unlike earlier models that often achieve only partial identifiability of latent coupled variables, *e.g.*, latent content variables but not latent style variables (Daunhawer et al., 2023), our model extends this scope to ensure complete identifiability of coupled variables. This comprehensive identifiability result allows for a more complete understanding and representation of the data. b) (Depth of Identifiability) In terms of depth, our model provides a more nuanced and detailed analysis by identifying coupled variables up to linear or permutation transformations. This level of precision offers an enhancement over the block identifiability approach typically seen in previous studies (Daunhawer et al., 2023; Yao et al., 2023), allowing for learning disentangled representations. We will further clarify this in section 4.

3. Identifiability Analysis

In this section, we conduct an identifiability analysis for the proposed latent partial causal model illustrated in Figure 1. Our analysis specifically focuses on two distinct types of latent spaces: the hypersphere and convex bodies, which are explored under certain defined assumptions.

3.1. Identifiability Analysis on Hypersphere

On hypersphere, we parameterize the proposed latent partial causal generative models depicted in Figure 1 by the following:

$$p(\mathbf{z}_x) = |\mathcal{Z}|^{-1}, \quad p(\mathbf{z}_t|\mathbf{z}_x) = C_p e^{(k\mathbf{z}_t^T \mathbf{z}_x)}, \quad (4)$$

$$\mathbf{x} = \mathbf{g}_x(\mathbf{z}_x, \mathbf{m}_x), \quad \mathbf{t} = \mathbf{g}_t(\mathbf{z}_t, \mathbf{m}_t), \quad (5)$$

where \mathcal{Z} denotes the space of latent factors \mathbf{z}_x and \mathbf{z}_t . Influenced by the commonly used feature normalization in contrastive loss, we assume that \mathcal{Z} is the unit hypersphere \mathbb{S}^{M-1} . We do not enforce any further assumptions for \mathbf{m}_x and \mathbf{m}_t . For \mathbf{g}_x and \mathbf{g}_t , we assume them to be invertible (*i.e.*, injective) mapping, ensuring the information in latent space can be recovered. In addition, we assume that $p(\mathbf{z}_x)$ follows a uniform distribution, and $p(\mathbf{z}_t|\mathbf{z}_x)$ follows a von Mises-Fisher (vMF) distribution, considering the constraint of unit hypersphere.

Given the aforementioned assumptions, our subsequent discussion aims to establish that the minimization of the symmetric contrastive loss (as defined in Equation (2)) converges to a symmetric cross entropy, as follows:

Theorem 3.1. (*\mathcal{L} converges to the symmetric cross-entropy*) Under the assumptions defined in Eq. (4)-(5) for the proposed latent partial causal model, the necessary condition $\mathbf{f}_x \circ \mathbf{g}_x = \mathbf{f}_t \circ \mathbf{g}_t$, denoted as \mathbf{h} , for the optimal normalized symmetric contrastive loss given by Eq. (2) leads to the following reduction of the loss itself:

$$\lim_{N \rightarrow \infty} \mathcal{L} - 2 \log N = \mathbb{E}_{\mathbf{z}_x \sim p(\mathbf{z}_x)} [H(p(\mathbf{z}_t|\mathbf{z}_x)), q_{\mathbf{h}}(\mathbf{z}_t|\mathbf{z}_x)] + \mathbb{E}_{\mathbf{z}_t \sim p(\mathbf{z}_t)} [H(p(\mathbf{z}_x|\mathbf{z}_t)), q_{\mathbf{h}}(\mathbf{z}_x|\mathbf{z}_t)], \quad (6)$$

where H is the cross entropy, the conditional distributions $q_{\mathbf{h}}(\mathbf{z}_t|\mathbf{z}_x)$ and $q(\mathbf{z}_x|\mathbf{z}_t)$ are parameterized by the following:

$$q_{\mathbf{h}}(\mathbf{z}_x|\mathbf{z}_t) = C_q(\mathbf{z}_t) e^{(\mathbf{h}(\mathbf{z}_x)^T \mathbf{h}(\mathbf{z}_t)/\tau)}, \quad (7)$$

$$q_{\mathbf{h}}(\mathbf{z}_t|\mathbf{z}_x) = C_q(\mathbf{z}_x) e^{(\mathbf{h}(\mathbf{z}_t)^T \mathbf{h}(\mathbf{z}_x)/\tau)}, \quad (8)$$

with

$$C_q(\mathbf{z}_t) = \int e^{(\mathbf{h}(\mathbf{z}_x)^T \mathbf{h}(\mathbf{z}_t)/\tau)} d\mathbf{z}_x,$$

$$C_q(\mathbf{z}_x) = \int e^{(\mathbf{h}(\mathbf{z}_x)^T \mathbf{h}(\mathbf{z}_t)/\tau)} d\mathbf{z}_t.$$

Proof sketch The proof can be done by the following three distinct steps, each building upon the previous one. Initially, we establish that the minimization of the right-hand side of Eq. (2) implies the following necessary condition: $\mathbf{f}_x \circ \mathbf{g}_x(\mathbf{m}_x, \mathbf{z}_x) = \mathbf{f}_t \circ \mathbf{g}_t(\mathbf{m}_t, \mathbf{z}_t)$ for all real pairs $((\mathbf{m}_x, \mathbf{z}_x), (\mathbf{m}_t, \mathbf{z}_t))$. In the second step, utilizing the necessary condition and the conditional distribution defined in

Eq. (4), we demonstrate that $\mathbf{f}_x \circ \mathbf{g}_x = \mathbf{f}_t \circ \mathbf{g}_t$, defined as \mathbf{h} , and they are independent of the variables \mathbf{m}_x and \mathbf{m}_t , which confirms that Eq. (7) and Eq. (8) do not depend on modality-specific latent variables \mathbf{m}_x and \mathbf{m}_t . Finally, the third step concludes our result by introducing the inference model Eqs. (7)-(8). See Appendix A.4.1 for details.

Identifiability Discussion Theorem 3.1 builds upon and extends the findings of Theorem 1 as presented in Zimmermann et al. (2021) to multi-modal context. Specifically, within a single-modal context, Theorem 3.1 aligns with the result outlined in Theorem 1 of Zimmermann et al. (2021). This advancement facilitates the application of Propositions 1 and 2 from Zimmermann et al. (2021) to multimodal contrastive representation learning. As a result, we can demonstrate that the minimization of Equation (6) in Theorem 3.1 is capable of identifying the latent variables \mathbf{z}_x and \mathbf{z}_t up to a linear transformation, *i.e.*, the recovered latent variable $\hat{\mathbf{z}}_x$, obtained through the minimization of Equation (6), is linearly related to the true \mathbf{z}_x as follows: $\hat{\mathbf{z}}_x = \mathbf{A}\mathbf{z}_x + \mathbf{c}$, where \mathbf{A} represents an orthogonal matrix, and \mathbf{c} is a constant vector. The comprehensive proof supporting this statement can be found in Appendix for completeness A.4.2.

The identifiability result above enables the extraction of independent latent variables through linear ICA after acquiring the recovered latent variables $\hat{\mathbf{z}}$. It is essential to acknowledge the geometric constraints imposed by the hypersphere setting. While it may not be feasible for all components of \mathbf{z} to be independent, a subset of \mathbf{z} can still exhibit independence. The extraction of these independent subsets is significant for investigating the capability of disentanglement. Further details on this subject will be thoroughly explored in Section 4.

3.2. Identifiability Analysis on convex bodies

The previous theoretical result requires the latent coupled variables to be a hypersphere, this will limit the disentangled ability of multimodal contrastive representation learning, due to the nature of the geometric constraints on the hypersphere. In this section, we will show a similar result for convex bodies, *e.g.*, the hyperrectangle $[a_1, b_1] \times \dots \times [a_M, b_M]$, which allows for independence among the latent coupled variables, offering a more flexible framework.

On convex bodies, we parameterize the proposed latent partial causal generative models depicted in Figure 1 by the following:

$$p(\mathbf{z}_x) = |\mathcal{Z}_c|^{-1}, \quad p(\mathbf{z}_t|\mathbf{z}_x) = C_p(\mathbf{z}_x)e^{-\delta(\mathbf{z}_t, \mathbf{z}_x)/\lambda}, \quad (9)$$

$$\mathbf{x} = \mathbf{g}_x(\mathbf{z}_x, \mathbf{m}_x), \quad \mathbf{t} = \mathbf{g}_t(\mathbf{z}_t, \mathbf{m}_t), \quad (10)$$

where δ is a distance metric induced by a norm (See Appendix A.5.2). Diverging from the hypersphere space mentioned above, here we consider a convex body in \mathbb{R}^M , de-

noted as \mathcal{Z}_c . In this context, we assume that $p(\mathbf{z}_x)$ follows a uniform distribution, and the conditional distribution $p(\mathbf{z}_t|\mathbf{z}_x)$ follows an exponential distribution as defined in Eq. (9). Again, we do not enforce any further assumptions for \mathbf{m}_x and \mathbf{m}_t . For \mathbf{g}_x and \mathbf{g}_t , we assume them to be invertible mapping, ensuring information in latent space can be recovered. Given these assumptions on a convex body, similar to Theorem 3.1 on hypersphere, we have the following result:

Theorem 3.2. (*\mathcal{L} converges to the symmetric cross-entropy*) Under the assumptions defined in Eq. (9)-(10) for the proposed latent partial causal model, the necessary condition $\mathbf{f}_x \circ \mathbf{g}_x = \mathbf{f}_t \circ \mathbf{g}_t$, denoted as \mathbf{h} , for the optimal normalized symmetric contrastive loss given by Eq. (2) leads to the following reduction of the loss itself:

$$\lim_{N \rightarrow \infty} \mathcal{L} - 2 \log N = \mathbb{E}_{\mathbf{z}_x \sim p(\mathbf{z}_x)} [H(p(\mathbf{z}_t|\mathbf{z}_x)), q_{\mathbf{h}}(\mathbf{z}_t|\mathbf{z}_x)] + \mathbb{E}_{\mathbf{z}_t \sim p(\mathbf{z}_t)} [H(p(\mathbf{z}_x|\mathbf{z}_t)), q_{\mathbf{h}}(\mathbf{z}_x|\mathbf{z}_t)] \quad (11)$$

where H is the cross entropy, the conditional distributions $q_{\mathbf{h}}(\mathbf{z}_t|\mathbf{z}_x)$ and $q(\mathbf{z}_x|\mathbf{z}_t)$ are parameterized by the following:

$$q_{\mathbf{h}}(\mathbf{z}_x|\mathbf{z}_t) = C_q(\mathbf{z}_t)e^{-\delta(\mathbf{h}(\mathbf{z}_x), \mathbf{h}(\mathbf{z}_t))/\tau}, \quad (12)$$

$$q_{\mathbf{h}}(\mathbf{z}_t|\mathbf{z}_x) = C_q(\mathbf{z}_x)e^{-\delta(\mathbf{h}(\mathbf{z}_x), \mathbf{h}(\mathbf{z}_t))/\tau}, \quad (13)$$

with

$$C_q(\mathbf{z}_t) = \int e^{-\delta(\mathbf{h}(\mathbf{z}_x), \mathbf{h}(\mathbf{z}_t))/\tau} d\mathbf{z}_x,$$

$$C_q(\mathbf{z}_x) = \int e^{-\delta(\mathbf{h}(\mathbf{z}_x), \mathbf{h}(\mathbf{z}_t))/\tau} d\mathbf{z}_t.$$

Proof sketch Similar to Proof sketch for theorem 3.1. Firstly, we demonstrate that by minimizing Eq. (2), the following necessary condition holds: $\mathbf{f}_x \circ \mathbf{g}_x(\mathbf{m}_x, \mathbf{z}_x) = \mathbf{f}_t \circ \mathbf{g}_t(\mathbf{m}_t, \mathbf{z}_t)$ holds for all pairs $((\mathbf{m}_x, \mathbf{z}_x), (\mathbf{m}_t, \mathbf{z}_t))$. Next, based on the condition, we show that $\mathbf{f}_x \circ \mathbf{g}_x = \mathbf{f}_t \circ \mathbf{g}_t$, defined as \mathbf{h} , and they are independent of the variables \mathbf{m}_x and \mathbf{m}_t , which enables Eq. (12) and Eq. (13) not depending on modality-specific latent variables \mathbf{m}_x and \mathbf{m}_t . Finally, the third step concludes our proof by introducing the model Eqs. (12)-(13). See Appendix A.5.1 for details.

Identifiability Discussion Theorem 3.2 extends the findings of Theorem 5 in Zimmermann et al. (2021). Again, in the context of a single-modal setting, Theorem 3.1 is consistent with the results of Theorem 5 as stated in Zimmermann et al. (2021). Given this, we can easily demonstrate that Eq. (11) in theorem 3.2 can identify the latent variables \mathbf{z}_x and \mathbf{z}_t up to a permutation transformation, *i.e.*, the recovered latent variable $\hat{\mathbf{z}}_x$, obtained through the minimization of Equation (6), is linearly related to the true \mathbf{z}_x as follows: $\hat{\mathbf{z}}_x = \mathbf{P}\mathbf{z}_x + \mathbf{c}$, where \mathbf{P} represents an orthogonal matrix,

and \mathbf{c} is a constant vector, by using Theorem 6 in Zimmermann et al. (2021). For completeness, the detailed proof of this assertion is provided in Appendix A.5.2.

4. Learning Disentangled Representations

Building on the foundation laid by our identifiability results, we now shift our focus to investigating the disentanglement ability by multimodal contrastive representation learning. Recognizing that training a model from scratch could be time-consuming and resource-intensive, we turn our attention to the disentanglement potential of the pre-trained multimodal model, *e.g.*, CLIP. In this section, we propose two distinct methods, guided by our identifiability results, for exploring the disentanglement ability of the pre-trained CLIP model. These two methods are tailored to suit the different latent space settings of hypersphere space and convex bodies.

On hypersphere Theorem 3.1 suggests that minimizing Eq. (6), in alignment with the standard training process of the CLIP model, enables the identification of latent variables \mathbf{z}_x up to linear transformations. This is significant as it facilitates the extraction of independent latent variables from features acquired via a pre-trained CLIP model, further processed using linear ICA methods. An important consideration is the geometric constraints inherent to the hypersphere, particularly for a unit $M - 1$ hypersphere. In this context, the maximum number of independent dimensions that can define each point on the hypersphere is $M - 1$. Consequently, the latent variables \mathbf{z}_x are limited to having at most $M - 1$ independent dimensions. In the extreme situation, all true latent variables \mathbf{z}_x might be dependent. Even in such scenarios, linear ICA methods may be still effective, since it is designed to extract components or features with maximum independence, utilizing the principle of maximal non-gaussianity (Hyvärinen et al., 2001). In our implementation, we employ the FastICA method proposed in Hyvärinen (1999).

On convex bodies Unlike a hypersphere space, a convex body provides the flexibility to have independent latent variables \mathbf{z}_x . Our Theorem 3.2 demonstrates that, by minimizing Eq. (6) within a convex body setting, we can identify these latent variables \mathbf{z}_x up to permutation. However, there exists a discrepancy: the CLIP model is originally trained in a hypersphere space, which inherently differs from the convex body assumptions foundational to Theorem 3.2. Despite this divergence, the pre-trained CLIP model may still be effective, since it, essentially, still aligns correct pairs and distances incorrect ones. It is important to note that the essential factor in achieving permutation identifiability through the minimization of Eq. (6) is the property of isometry in the mapping \mathbf{h} in Theorem 3.2. Although a

global isometric mapping from a convex body to a whole hypersphere is not feasible, the existence of a local and approximate isometry from a convex body to a small region on the hypersphere is a plausible consideration. Taking this into account, we can utilize Principal Component Analysis (PCA) to process the features learned by the pre-trained CLIP model, effectively reducing redundant information on the hypersphere. Subsequently, FastICA can be applied to counteract the orthogonal transformation effect introduced by PCA, thereby extracting the final features.

5. Experiments

Experiments on Synthetic Data In our initial experiments, we use synthetic data to verify our main identifiability results on hypersphere and convex bodies, and empirically demonstrate the robustness of these results when facing substantial violations of assumptions. The synthetic data is generated through a specific process as the following. We consider latent coupled variables \mathbf{z}_x and \mathbf{z}_t , each with a dimensionality of 10. Additionally, we have modality-specific latent variables \mathbf{m}_x and \mathbf{m}_t , both set to a dimension of 5. The process begins with sampling from the marginal distribution $p(\mathbf{z}_x)$. We explore this both under conditions that align with our theoretical assumptions (using uniform distributions) and under conditions that deviate from these assumptions (using non-uniform distributions). We then create real pairs by sampling from the conditional distribution $p(\mathbf{z}_t|\mathbf{z}_x)$. This is done in two different settings: one that matches our assumptions about the conditional distribution and one that violates these assumptions. The observational data \mathbf{x} and \mathbf{t} are generated using two different 3-layer Multi-Layer Perceptrons (MLPs) with leaky ReLU units. Both sets of modality-specific latent variables, \mathbf{m}_x and \mathbf{m}_t , are independently sampled from a Gaussian distribution. Beyond the hypersphere space, our experiments also encompass the bounded box (a type of convex body) and unbounded space.

To test for identifiability up to linear transformations formalized by Theorem 3.1, we fit a linear regression model between the ground-truth \mathbf{z}_x and recovered $\hat{\mathbf{z}}_x$ and report the coefficient of determination (R^2). Further, to test for identifiability up to permutations formalized by theorem 3.2, we employ the mean correlation coefficient (MCC). The first row in Table 1 and the first two rows in Table 2, corresponding to the setting where the assumptions are satisfied, verify the identifiability results on hypersphere and convex bodies, respectively. Our empirical investigations have yielded a critical insight: discrepancies in the assumptions concerning marginal and conditional distributions, as well as the nature of the spaces (hypersphere and convex body), do not significantly impact performance. This robustness is demonstrated by the results detailed in Table 1 for the

Revealing Multimodal Contrastive Representation Learning through Latent Partial Causal Models

Table 1. Assessing identifiability up to linear transformations under varying assumptions. The first row corresponds to a setting that matches our assumptions in theorem 3.1, while the others show results for violated assumptions. S: Space, Sp: Sphere, U: Uniform, v: vMF ($k = 1$), L: Laplace ($\lambda = 0.05$), N: Normal ($\delta = 0.05$), B: Box, Un: Unbounded, G: GenNorm($\beta = 3$)

Generative process			Model		R2
S	$p(\mathbf{z}_x)$	$p(\mathbf{z}_x \mathbf{z}_t)$	S	$q(\mathbf{z}_x \mathbf{z}_t)$	
Sp	U	v	Sp	v	99.5 ± 0.1
Sp	U	L	Sp	v	99.4 ± 0.2
Sp	U	N	Sp	v	98.7 ± 0.3
B	U	N	Un	N	90.5 ± 0.2
B	U	L	Un	N	92.2 ± 0.3
B	U	L	Un	G	99.1 ± 0.4
B	U	N	Un	G	91.2 ± 0.3
Sp	N ($\delta = 1$)	L	Sp	v	96.3 ± 0.3
Sp	N ($\delta = 1$)	N	Sp	v	95.9 ± 0.2
Un	L ($\lambda = 1$)	N	Un	N	88.5 ± 0.3
Un	N ($\delta = 1$)	N	Un	N	89.2 ± 0.2

Table 2. Assessing identifiability up to permutation under varying assumptions. The first two rows correspond to a setting that matches our assumptions in theorem 3.2, while the others show results for violated assumptions. S: Space, Sp: Sphere, U: Uniform, v: vMF ($k = 1$), L: Laplace ($\lambda = 0.05$), N: Normal ($\delta = 0.05$), B: Box, Un: Unbounded, G: GenNorm ($\beta = 3, \lambda = 0.05$)

Generative process			Model		MCC
S	$p(\mathbf{z}_x)$	$p(\mathbf{z}_x \mathbf{z}_t)$	S	$q(\mathbf{z}_x \mathbf{z}_t)$	
B	U	L	B	L	99.1 ± 0.1
B	U	G	B	G	97.2 ± 0.3
B	U	N	B	N	98.6 ± 0.2
B	U	L	B	N	99.1 ± 0.1
B	U	G	B	L	98.4 ± 0.1
B	U	L	Un	L	95.6 ± 0.2
B	U	G	Un	G	96.4 ± 0.2

hypersphere space and Table 2 for convex bodies. This observation is similar to reports from studies conducted in the context of single-model context (Zimmermann et al., 2021). This observation might be attributed to the fact that the loss function described in Eq. 2 predominantly relies on the computation of expectations, inherently allowing for a wide range of approximations. If we can approximate the expectation calculations consistently across various distributions and spaces, it is reasonable to expect that the identifiability results remain well within acceptable bounds.

Disentangled representations for CelebA data Informed by our identifiability results and the empirical evidence presented earlier, we have grounds to claim that the pre-trained CLIP model possesses disentanglement ability. To substantiate this, as discussed in Section 4, we first extract features from the pre-trained CLIP model and then apply FastICA to these features to achieve final representations. We expect these final representations to exhibit clear signs of disentanglement. To validate this, we proceed to train

a decoder that reconstructs observational data using these extracted representations. We implement the above process on the CelebA face dataset (Liu et al., 2015), which has been explored by previous studies to learn disentangled representations (Kim & Mnih, 2018; Chen et al., 2018).

Figure 2 illustrates the effectiveness of our method through latent space traversals. Specifically, it visualizes changes in reconstructions as we traverse one dimension of the latent space at a time, showcasing 4 out of 16 attributes uncovered by our approach. Our method yields competitive results when compared with specialized techniques for learning disentangled representations, such as FactorVAE (Kim & Mnih, 2018) and β -TCVAE (Chen et al., 2018). As reported, FactorVAE identified 8 disentangled attributes and β -TCVAE reported 15, our method successfully discerns 16 distinct disentangled representations. Additional results are available in Appendix A.6. This achievement not only underscores the effectiveness of our method and validates our identifiability results, but also offers new perspectives and insights into learning disentangled representations by pre-trained CLIP.

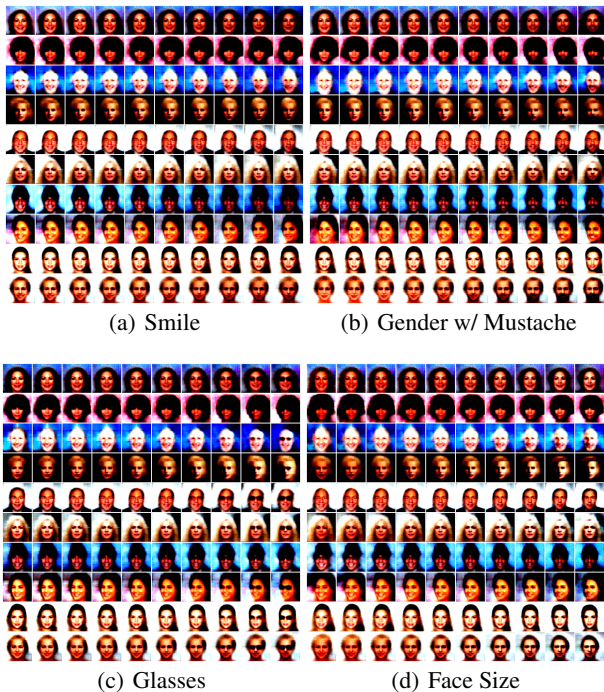


Figure 2. Disentangled Representations learned by combining pre-train CLIP and FastICA. The proposed method obtains 16 disentangled representations, refer to Appendix A.6 for more results.

Few-shot learning and domain generalization on ImageNet-type data Broadly, the objective of disentangled representations is to learn features that lend themselves to be easily and robustly transferred to downstream tasks. This implies that disentangled representations should inherently possess a satisfactory capability for few-shot learn-

Table 3. Quantitative results for 2-shot transfer learning and domain generalization by different methods. Lin. P. (Linear Probe).

ENCODERS	METHODS	SOURCE		TARGET (IMAGENET-)			
		IMAGENET	V2	SKETCH	R	A	AVG.
RN50	LIN. P.	31.95	26.48	8.41	20.74	7.44	15.77
	LIN. P. w/ FASTICA	34.06	28.74	8.37	21.72	10.15	17.25
	LIN. P. w/ PCA AND FASTICA	34.12	28.68	11.55	25.57	10.15	18.99
RN101	LIN. P.	37.64	31.45	13.71	31.09	11.85	20.03
	LIN. P. w/ FASTICA	39.58	33.15	13.49	30.29	14.77	22.93
	LIN. P. w/ PCA AND FASTICA	39.86	33.58	17.93	35.48	14.20	25.29
ViT32	LIN. P.	38.23	32.00	16.17	33.67	12.88	23.68
	LIN. P. w/ FASTICA	40.21	33.97	16.54	34.79	15.72	25.26
	LIN. P. w/ PCA AND FASTICA	39.34	33.44	19.02	36.98	14.69	26.03
ViT16	LIN. P.	44.97	38.11	22.06	43.86	25.99	32.51
	LIN. P. w/ FASTICA	45.52	39.38	22.55	45.33	30.47	34.43
	LIN. P. w/ PCA AND FASTICA	46.57	40.66	26.67	49.69	31.48	37.13

Table 4. Quantitative results for 4-shot transfer learning and domain generalization by different methods. Lin. P. (Linear Probe).

ENCODERS	METHODS	SOURCE		TARGET (IMAGENET-)			
		IMAGENET	V2	SKETCH	R	A	AVG.
RN50	LIN. P.	41.34	33.67	11.55	26.27	9.67	20.29
	LIN. P. w/ FASTICA	44.10	36.07	12.75	30.15	11.64	22.65
	LIN. P. w/ PCA AND FASTICA	42.86	35.38	12.29	28.81	9.79	21.57
RN101	LIN. P.	48.23	39.53	18.80	38.10	14.32	27.69
	LIN. P. w/ FASTICA	49.43	41.02	17.49	39.33	15.25	28.27
	LIN. P. w/ PCA AND FASTICA	49.01	40.25	19.26	39.71	14.75	28.49
ViT32	LIN. P.	47.82	39.53	21.51	40.94	15.99	29.49
	LIN. P. w/ FASTICA	49.43	40.66	22.66	41.78	16.41	30.38
	LIN. P. w/ PCA AND FASTICA	49.48	41.09	23.72	43.48	16.77	31.27
ViT16	LIN. P.	54.30	46.06	27.58	50.76	29.24	38.41
	LIN. P. w/ FASTICA	56.65	48.18	28.27	55.50	33.39	41.33
	LIN. P. w/ PCA AND FASTICA	56.16	47.46	30.21	55.49	31.71	41.22

ing and demonstrate robustness against distribution shifts. Therefore, we focus on tasks involving few-shot learning and domain generalization, to validate our identifiability results and the efficacy of the proposed methods. To achieve this, we first obtain representations of a limited set of labeled samples. This is done either by utilizing the pre-trained CLIP model followed by FastICA (labeled as Linear Probe with FastICA, applied within the hypersphere space) or by employing the pre-trained CLIP model in conjunction with PCA and FastICA (labeled as Linear Probe with PCA and FastICA, aligning with convex bodies). These extracted representations, along with their labels, are used to train a linear classifier. We train the proposed methods on ImageNet (Deng et al., 2009) with limited samples to evaluate their performance for few-shot learning, and also conduct evaluations on ImageNet-V2 (Recht et al., 2019), ImageNet-Sketch (Wang et al., 2019), ImageNet-R (Hendrycks et al., 2021a), and ImageNet-A (Hendrycks et al., 2021b) for demonstrating the robustness to distribution shift.

Tables 3 and 4 present the performance metrics of the proposed methods in few-shot learning scenarios (as shown in the ‘SOURCE’ column) and in the context of distribution shift (as indicated in the ‘TARGET’ columns). An analysis of the data for the ‘SOURCE’ column in these tables reveals

that the proposed methods outperform the baseline approach of training a linear classifier with features directly obtained from pre-trained CLIP, known as Linear Probe. This superior performance underscores the enhanced adaptability of our proposed methods, particularly in tasks requiring rapid learning from limited data. Furthermore, observations from the ‘TARGET’ column demonstrate that our proposed methods also surpass the Linear Probe approach in terms of distribution shift, which affirms the robustness of our methods. See Appendix A.7 for more results.

6. Conclusion

In this study, we demonstrate that multimodal contrastive representation learning can effectively identify latent coupled variables up to a linear transformation on the hypersphere and up to permutation on convex bodies. This insight significantly contributes to our understanding of the success factors behind multimodal contrastive representation learning. Building on these theoretical findings, we investigate the disentanglement ability of pre-trained multimodal models such as CLIP, each tailored to different spaces. Our experiments with synthetic data not only corroborate our theoretical assertions but also empirically show that the identifiability results remain valid even when various assumptions are not met. Further, our experiments on the CelebA dataset,

few-shot learning, and domain generalization, highlight the potential for learning disentangled representations by pre-trained CLIP. While our findings are promising, the pursuit of even more effective methods to unlock and harness the full potential of disentanglement in pre-trained CLIP models remains a valuable and ongoing endeavor.

7. Impact Statement

This paper presents work whose goal is to advance the field of Machine Learning. There are many potential societal consequences of our work, none of which we feel must be specifically highlighted here.

References

- Ban, Y. and Dong, Y. Pre-trained adversarial perturbations. *Advances in Neural Information Processing Systems*, 35: 1196–1209, 2022.
- Chen, R. T., Li, X., Grosse, R. B., and Duvenaud, D. K. Isolating sources of disentanglement in variational autoencoders. *Advances in neural information processing systems*, 31, 2018.
- Chen, T., Kornblith, S., Norouzi, M., and Hinton, G. A simple framework for contrastive learning of visual representations. In *International conference on machine learning*, pp. 1597–1607. PMLR, 2020.
- Daunhawer, I., Bizeul, A., Palumbo, E., Marx, A., and Vogt, J. E. Identifiability results for multimodal contrastive learning. *arXiv preprint arXiv:2303.09166*, 2023.
- Deng, J., Dong, W., Socher, R., Li, L.-J., Li, K., and Fei-Fei, L. Imagenet: A large-scale hierarchical image database. In *2009 IEEE conference on computer vision and pattern recognition*, pp. 248–255. Ieee, 2009.
- Fidler, S., Sharma, A., and Urtasun, R. A sentence is worth a thousand pixels. In *Proceedings of the IEEE conference on Computer Vision and Pattern Recognition*, pp. 1995–2002, 2013.
- Gresele, L., Rubenstein, P. K., Mehrjou, A., Locatello, F., and Schölkopf, B. The incomplete rosetta stone problem: Identifiability results for multi-view nonlinear ica. In *Uncertainty in Artificial Intelligence*, pp. 217–227. PMLR, 2020.
- Gropper, G. L. Why is a picture worth a thousand words? *Audio Visual Communication Review*, 11(4):75–95, 1963.
- Gutmann, M. and Hyvärinen, A. Noise-contrastive estimation: A new estimation principle for unnormalized statistical models. In *Proceedings of the thirteenth international conference on artificial intelligence and statistics*, pp. 297–304. JMLR Workshop and Conference Proceedings, 2010.
- He, K., Fan, H., Wu, Y., Xie, S., and Girshick, R. Momentum contrast for unsupervised visual representation learning. In *Proceedings of the IEEE/CVF conference on computer vision and pattern recognition*, pp. 9729–9738, 2020.
- He, X. and Peng, Y. Fine-grained image classification via combining vision and language. In *Proceedings of the IEEE Conference on Computer Vision and Pattern Recognition*, pp. 5994–6002, 2017.
- Hendrycks, D., Basart, S., Mu, N., Kadavath, S., Wang, F., Dorundo, E., Desai, R., Zhu, T., Parajuli, S., Guo, M., Song, D., Steinhardt, J., and Gilmer, J. The many faces of robustness: A critical analysis of out-of-distribution generalization. *ICCV*, 2021a.
- Hendrycks, D., Zhao, K., Basart, S., Steinhardt, J., and Song, D. Natural adversarial examples. *CVPR*, 2021b.
- Huang, Y., Du, C., Xue, Z., Chen, X., Zhao, H., and Huang, L. What makes multi-modal learning better than single (provably). *Advances in Neural Information Processing Systems*, 34:10944–10956, 2021.
- Hum, N. J., Chamberlin, P. E., Hambright, B. L., Portwood, A. C., Schat, A. C., and Bevan, J. L. A picture is worth a thousand words: A content analysis of facebook profile photographs. *Computers in Human Behavior*, 27(5):1828–1833, 2011.
- Hyvarinen, A. Fast and robust fixed-point algorithms for independent component analysis. *IEEE transactions on Neural Networks*, 10(3):626–634, 1999.
- Hyvarinen, A. and Morioka, H. Unsupervised feature extraction by time-contrastive learning and nonlinear ica. *Advances in neural information processing systems*, 29, 2016.
- Hyvarinen, A. and Morioka, H. Nonlinear ica of temporally dependent stationary sources. In *Artificial Intelligence and Statistics*, pp. 460–469. PMLR, 2017.
- Hyvärinen, A. and Pajunen, P. Nonlinear independent component analysis: Existence and uniqueness results. *Neural networks*, 12(3):429–439, 1999.
- Hyvärinen, A., Karhunen, J., and Oja, E. *Independent Component Analysis*. Adaptive and Cognitive Dynamic Systems: Signal Processing, Learning, Communications and Control. Wiley, 2001.
- Hyvarinen, A., Sasaki, H., and Turner, R. Nonlinear ica using auxiliary variables and generalized contrastive learning. In *The 22nd International Conference on Artificial Intelligence and Statistics*, pp. 859–868. PMLR, 2019.

- Jiang, H. Uniform convergence rates for kernel density estimation. In *International Conference on Machine Learning*, pp. 1694–1703. PMLR, 2017.
- Khemakhem, I., Kingma, D., Monti, R., and Hyvarinen, A. Variational autoencoders and nonlinear ica: A unifying framework. In *International Conference on Artificial Intelligence and Statistics*, pp. 2207–2217. PMLR, 2020.
- Kim, H. and Mnih, A. Disentangling by factorising. In *International Conference on Machine Learning*, pp. 2649–2658. PMLR, 2018.
- Liang, V. W., Zhang, Y., Kwon, Y., Yeung, S., and Zou, J. Y. Mind the gap: Understanding the modality gap in multi-modal contrastive representation learning. *Advances in Neural Information Processing Systems*, 35: 17612–17625, 2022.
- Liu, Z., Luo, P., Wang, X., and Tang, X. Deep learning face attributes in the wild. In *Proceedings of International Conference on Computer Vision (ICCV)*, December 2015.
- Lüddecke, T. and Ecker, A. Image segmentation using text and image prompts. In *Proceedings of the IEEE/CVF Conference on Computer Vision and Pattern Recognition*, pp. 7086–7096, 2022.
- Mori, Y., Takahashi, H., and Oka, R. Image-to-word transformation based on dividing and vector quantizing images with words. In *First international workshop on multimedia intelligent storage and retrieval management*, pp. 1–9. Citeseer, 1999.
- Nakada, R., Gulluk, H. I., Deng, Z., Ji, W., Zou, J., and Zhang, L. Understanding multimodal contrastive learning and incorporating unpaired data. In *International Conference on Artificial Intelligence and Statistics*, pp. 4348–4380. PMLR, 2023.
- Oord, A. v. d., Li, Y., and Vinyals, O. Representation learning with contrastive predictive coding. *arXiv preprint arXiv:1807.03748*, 2018.
- Quattoni, A., Collins, M., and Darrell, T. Learning visual representations using images with captions. In *2007 IEEE Conference on Computer Vision and Pattern Recognition*, pp. 1–8. IEEE, 2007.
- Radford, A., Kim, J. W., Hallacy, C., Ramesh, A., Goh, G., Agarwal, S., Sastry, G., Askell, A., Mishkin, P., Clark, J., et al. Learning transferable visual models from natural language supervision. In *International conference on machine learning*, pp. 8748–8763. PMLR, 2021.
- Ramanathan, V., Liang, P., and Fei-Fei, L. Video event understanding using natural language descriptions. In *Proceedings of the IEEE international conference on computer vision*, pp. 905–912, 2013.
- Recht, B., Roelofs, R., Schmidt, L., and Shankar, V. Do imagenet classifiers generalize to imagenet? In *International conference on machine learning*, pp. 5389–5400. PMLR, 2019.
- Reinert, H. One picture is worth a thousand words? not necessarily! *Modern Language Journal*, pp. 160–168, 1976.
- Rojas-Carulla, M., Schölkopf, B., Turner, R., and Peters, J. Invariant models for causal transfer learning. *The Journal of Machine Learning Research*, 19(1):1309–1342, 2018.
- Saunshi, N., Plevrakis, O., Arora, S., Khodak, M., and Khandeparkar, H. A theoretical analysis of contrastive unsupervised representation learning. In *International Conference on Machine Learning*, pp. 5628–5637. PMLR, 2019.
- Schölkopf, B., Locatello, F., Bauer, S., Ke, N. R., Kalchbrenner, N., Goyal, A., and Bengio, Y. Toward causal representation learning. *Proceedings of the IEEE*, 109(5): 612–634, 2021.
- Shi, Y., Paige, B., Torr, P., et al. Variational mixture-of-experts autoencoders for multi-modal deep generative models. *Advances in neural information processing systems*, 32, 2019.
- Tian, Y., Krishnan, D., and Isola, P. Contrastive multiview coding. In *Computer Vision—ECCV 2020: 16th European Conference, Glasgow, UK, August 23–28, 2020, Proceedings, Part XI 16*, pp. 776–794. Springer, 2020.
- Von Kügelgen, J., Sharma, Y., Gresele, L., Brendel, W., Schölkopf, B., Besserve, M., and Locatello, F. Self-supervised learning with data augmentations provably isolates content from style. *Advances in neural information processing systems*, 34:16451–16467, 2021.
- Wang, H., Ge, S., Lipton, Z., and Xing, E. P. Learning robust global representations by penalizing local predictive power. In *Advances in Neural Information Processing Systems*, pp. 10506–10518, 2019.
- Wang, J., Markert, K., Everingham, M., et al. Learning models for object recognition from natural language descriptions. In *BMVC*, volume 1, pp. 2. Citeseer, 2009.
- Wang, T. and Isola, P. Understanding contrastive representation learning through alignment and uniformity on the hypersphere. In *International Conference on Machine Learning*, pp. 9929–9939. PMLR, 2020.
- Wu, Z., Xiong, Y., Yu, S. X., and Lin, D. Unsupervised feature learning via non-parametric instance discrimination. In *Proceedings of the IEEE conference on computer vision and pattern recognition*, pp. 3733–3742, 2018.

- Yao, D., Xu, D., Lachapelle, S., Magliacane, S., Taslakian, P., Martius, G., von Kügelgen, J., and Locatello, F. Multi-view causal representation learning with partial observability. *arXiv preprint arXiv:2311.04056*, 2023.
- Zhang, Y., Jiang, H., Miura, Y., Manning, C. D., and Langlotz, C. P. Contrastive learning of medical visual representations from paired images and text. In *Machine Learning for Healthcare Conference*, pp. 2–25. PMLR, 2022.
- Zhou, K., Yang, J., Loy, C. C., and Liu, Z. Conditional prompt learning for vision-language models. In *Proceedings of the IEEE/CVF Conference on Computer Vision and Pattern Recognition*, pp. 16816–16825, 2022a.
- Zhou, K., Yang, J., Loy, C. C., and Liu, Z. Learning to prompt for vision-language models. *International Journal of Computer Vision*, 130(9):2337–2348, 2022b.
- Zimmermann, R. S., Sharma, Y., Schneider, S., Bethge, M., and Brendel, W. Contrastive learning inverts the data generating process. In *International Conference on Machine Learning*, pp. 12979–12990. PMLR, 2021.

A. Appendix

A.1. Related Work

Multimodal contrastive representation learning Multi-modal contrastive representation learning, driven by underlying co-occurrence patterns across various modalities, aims to coalesce inputs from these diverse sources into a cohesive representation space. This is typically achieved using a symmetric version of the standard contrastive loss (Oord et al., 2018; Gutmann & Hyvärinen, 2010), a method designed to align accurate pairings while distinguishing incorrect ones (He & Peng, 2017; Radford et al., 2021). Although this approach has proven successful in a range of downstream tasks (Radford et al., 2021; Zhou et al., 2022a;b; Lüddecke & Ecker, 2022; Ban & Dong, 2022), there remains a gap in our comprehensive theoretical and empirical understanding of the representations it learns. Recently, there has been a growing interest in exploring multi-modal contrastive learning from various perspectives. For instance, the study by Liang et al. (2022) provides insights into the modality gap inherent in multi-modal contrastive learning. Similarly, the research presented by Nakada et al. (2023) establishes a link between general multimodal contrastive loss and SVD analysis. Additionally, Huang et al. (2021) posits that learning with multiple modalities can lead to a reduced population risk compared to using a subset of these modalities. Diverging from these approaches, our work delves into multi-modal contrastive representation learning by examining its connection with generative models.

Past research has sought to comprehend the representations derived from standard single-modality contrastive learning, examining them through the lens of alignment and uniformity (Wang & Isola, 2020), showing guarantees on the performance of the learned representations on the average classification task (Saunshi et al., 2019), or in terms of the identifiability of latent variables (Zimmermann et al., 2021; Von Kügelgen et al., 2021). Building on these foundations, our work takes a foreword step. We demonstrate that multi-modal contrastive learning can identify latent coupled variables, extending the insights from previous studies into the realm of multi-modality.

Very recently, several studies have emerged, focusing on the intersection between the identifiability of latent variables and modal contrastive representation learning (Daunhawer et al., 2023; Gresele et al., 2020; Yao et al., 2023). Some of these works, however, have only achieved partial identifiability of coupled variables (Daunhawer et al., 2023; Yao et al., 2023), specifically identifying latent content variables but not latent style variables. In contrast, our work achieves comprehensive identifiability results for all latent coupled variables, offering a deeper level of understanding. Our research also diverges from the approach taken in (Gresele et al., 2020) in two key ways: Firstly, we model co-occurrence patterns using conditional distributions, whereas the latter utilizes identical variables for this purpose. Secondly, while (Gresele et al., 2020) relies on the premise that the mapping from the latent space to observations must be constrained by component-wise corrupters to ensure identifiability, our findings do not necessitate such constraints.

Nonlinear ICA Nonlinear Independent Component Analysis (ICA) aims to unravel latent independent variables from observational data that has been subject to a nonlinear mixture of these latent factors. However, as pointed out in the seminal work by Hyvärinen et al. (Hyvärinen & Pajunen, 1999), solving this problem is generally infeasible without specific underlying assumptions. A prominent direction in contemporary research leverages the concept of distributional changes in latent variables, which leads to the creation of multi-domain observational data. This approach has been extensively explored and developed in a series of studies (Hyvarinen & Morioka, 2016; 2017; Hyvarinen et al., 2019; Khemakhem et al., 2020), each contributing to a deeper understanding and more refined methodologies in the field of Nonlinear ICA. We build upon this body of research by incorporating co-occurrence patterns observed across multiple modalities. It is important to note the distinct difference between multi-domain and multi-modal approaches. The former typically implies a consistent mapping from the latent space to the observational space across all domains, whereas the latter accommodates different mappings for each modality. Additionally, while multi-domain approaches generally assume a totally shared latent variables across all domains, multi-modal methods allow for the existence of modality-specific latent variables.

A.2. The Proof of Theorem 2.1

Theorem 2.1. (The asymptotics of \mathcal{L}) For fixed $\tau > 0$, as the sample size $N \rightarrow \infty$, the (normalized) symmetric contrastive loss converges to

$$\begin{aligned} \lim_{N \rightarrow \infty} \mathcal{L} - 2 \log N = & -2 \mathbb{E}_{(\mathbf{x}, \mathbf{t}) \sim p(\mathbf{x}, \mathbf{t})} [d(\mathbf{f}_x(\mathbf{x}), \mathbf{f}_t(\mathbf{t})) / \tau] + \mathbb{E}_{\mathbf{x} \sim p(\mathbf{x})} \left[\log \mathbb{E}_{\mathbf{t} \sim p(\mathbf{t})} [e^{d(\mathbf{f}_x(\mathbf{x}), \mathbf{f}_t(\mathbf{t})) / \tau}] \right] \\ & + \mathbb{E}_{\mathbf{t} \sim p(\mathbf{t})} \left[\log \mathbb{E}_{\mathbf{x} \sim p(\mathbf{x})} [e^{d(\mathbf{f}_x(\mathbf{x}), \mathbf{f}_t(\mathbf{t})) / \tau}] \right]. \end{aligned} \quad (14)$$

Proof. This proof is done by extending the proof of Theorem 1 in Wang & Isola (2020), mainly depending on the Continuous Mapping Theorem and the law of large numbers.

$$\begin{aligned} \lim_{N \rightarrow \infty} \mathcal{L} = & \lim_{N \rightarrow \infty} \left(-\frac{1}{N} \sum_{i=1}^N \log \frac{e^{d(\mathbf{f}_x(\mathbf{x}_i), \mathbf{f}_t(\mathbf{t}_i)) / \tau}}{\sum_{j=1}^N e^{d(\mathbf{f}_x(\mathbf{x}_i), \mathbf{f}_t(\mathbf{t}_j)) / \tau}} - \frac{1}{N} \sum_{i=1}^N \log \frac{e^{d(\mathbf{f}_x(\mathbf{x}_i), \mathbf{f}_t(\mathbf{t}_i)) / \tau}}{\sum_{j=1}^N e^{d(\mathbf{f}_x(\mathbf{x}_j), \mathbf{f}_t(\mathbf{t}_i)) / \tau}} \right), \\ = & \lim_{N \rightarrow \infty} \left(-\frac{2}{N} \sum_{i=1}^N d(\mathbf{f}_x(\mathbf{x}_i), \mathbf{f}_t(\mathbf{t}_i)) / \tau + \frac{1}{N} \sum_{i=1}^N \log \sum_{j=1}^N e^{d(\mathbf{f}_x(\mathbf{x}_i), \mathbf{f}_t(\mathbf{t}_j)) / \tau} + \frac{1}{N} \sum_{i=1}^N \log \sum_{j=1}^N e^{d(\mathbf{f}_x(\mathbf{x}_j), \mathbf{f}_t(\mathbf{t}_i)) / \tau} \right) \\ = & \lim_{N \rightarrow \infty} \left(-\frac{2}{N} \sum_{i=1}^N d(\mathbf{f}_x(\mathbf{x}_i), \mathbf{f}_t(\mathbf{t}_i)) / \tau + \frac{1}{N} \sum_{i=1}^N \log \frac{1}{N} \sum_{j=1}^N e^{d(\mathbf{f}_x(\mathbf{x}_i), \mathbf{f}_t(\mathbf{t}_j)) / \tau} + \frac{1}{N} \sum_{i=1}^N \log \frac{1}{N} \sum_{j=1}^N e^{d(\mathbf{f}_x(\mathbf{x}_j), \mathbf{f}_t(\mathbf{t}_i)) / \tau} \right. \\ & \left. + \frac{2}{N} \sum_{i=1}^N \log N \right) \\ = & -2 \mathbb{E}_{(\mathbf{x}, \mathbf{t}) \sim p(\mathbf{x}, \mathbf{t})} [d(\mathbf{f}_x(\mathbf{x}), \mathbf{f}_t(\mathbf{t})) / \tau] + \mathbb{E}_{\mathbf{x} \sim p(\mathbf{x})} \left[\log \mathbb{E}_{\mathbf{t} \sim p(\mathbf{t})} [e^{d(\mathbf{f}_x(\mathbf{x}), \mathbf{f}_t(\mathbf{t})) / \tau}] \right] \\ & + \mathbb{E}_{\mathbf{t} \sim p(\mathbf{t})} \left[\log \mathbb{E}_{\mathbf{x} \sim p(\mathbf{x})} [e^{d(\mathbf{f}_x(\mathbf{x}), \mathbf{f}_t(\mathbf{t})) / \tau}] \right] + 2 \log N. \end{aligned}$$

□

A.3. Relation with Recovering All Information

In this section, we proof

$$\begin{aligned} & \mathbb{E}_{\mathbf{x} \sim p(\mathbf{x})} \left[\log \mathbb{E}_{\mathbf{t} \sim p(\mathbf{t})} [e^{d(\mathbf{f}_x(\mathbf{x}), \mathbf{f}_t(\mathbf{t})) / \tau}] \right] + \mathbb{E}_{\mathbf{t} \sim p(\mathbf{t})} \left[\log \mathbb{E}_{\mathbf{x} \sim p(\mathbf{x})} [e^{d(\mathbf{f}_x(\mathbf{x}), \mathbf{f}_t(\mathbf{t})) / \tau}] \right] \\ & \approx -H(p(\mathbf{f}_x(\mathbf{x})), p(\mathbf{f}_t(\mathbf{t}))) - H(p(\mathbf{f}_t(\mathbf{t})), p(\mathbf{f}_x(\mathbf{x}))). \end{aligned}$$

Considering the symmetry evident in both the left and right sides of the equation, let us focus our attention on the initial term on the left and its corresponding counterpart on the right.

$$\begin{aligned} & \mathbb{E}_{\mathbf{x} \sim p(\mathbf{x})} \left[\log \mathbb{E}_{\mathbf{t} \sim p(\mathbf{t})} [e^{d(\mathbf{f}_x(\mathbf{x}), \mathbf{f}_t(\mathbf{t})) / \tau}] \right] \\ = & \lim_{N \rightarrow \infty} \frac{1}{N} \sum_{i=1}^N \log \sum_{j=1}^N e^{d(\mathbf{f}_x(\mathbf{x}_i), \mathbf{f}_t(\mathbf{t}_j)) / \tau} \end{aligned} \quad (15)$$

$$\approx \lim_{N \rightarrow \infty} \frac{1}{N} \sum_{i=1}^N \log p_{\text{KDE}}(\mathbf{f}_x(\mathbf{x}_i)) + \log Z_{\text{KDE}} \quad (16)$$

$$= -H(p(\mathbf{f}_x(\mathbf{x}), p(\mathbf{f}_t(\mathbf{t}))) + \log Z_{\text{KDE}}, \quad (17)$$

Transitioning from Eq. (15) to Eq. (16), we employ kernel density estimation, wherein the choice of kernel is influenced by the distance metric used. For instance, on a hypersphere, a von Mises-Fisher kernel is suitable, whereas on convex bodies, a

Laplace kernel aligns well with the L1 norm. In this context, $\log Z_{\text{KDE}}$ represents the normalization constant associated with the kernel. The inherent symmetry in this setup allows us to logically deduce the equation. Note that since here the bandwidth τ can be optimized in multimodal contrastive representation learning, if true distribution is the same as the chosen kernel, Eq. (16) is equal to Eq. (15), *i.e.*, \approx in Eq. (16) can be $=$. Under certain conditions the kernel density estimation will converge to the real distribution, in that case \approx in Eq. (16) can also be $=$.

A.4. The Proof of identifiability on hypersphere

A.4.1. THE PROOF OF THEOREM 3.1

Theorem 3.1. (\mathcal{L} converges to the symmetric cross-entropy) *Under the assumptions defined in Eqs. (4)-(5) for the proposed latent partial causal model, the necessary condition $\mathbf{f}_x \circ \mathbf{g}_x = \mathbf{f}_t \circ \mathbf{g}_t$, denoted as \mathbf{h} , for the optimal normalized symmetric contrastive loss given by Eq. (2) leads to the following reduction of the loss itself:*

$$\lim_{N \rightarrow \infty} \mathcal{L} - 2 \log N = \mathbb{E}_{\mathbf{z}_x \sim p(\mathbf{z}_x)} [H(p(\mathbf{z}_t|\mathbf{z}_x), q_{\mathbf{h}}(\mathbf{z}_t|\mathbf{z}_x))] + \mathbb{E}_{\mathbf{z}_t \sim p(\mathbf{z}_t)} [H(p(\mathbf{z}_x|\mathbf{z}_t), q_{\mathbf{h}}(\mathbf{z}_x|\mathbf{z}_t))] \quad (18)$$

where H is the cross entropy, the conditional distributions $q_{\mathbf{h}}(\mathbf{z}_t|\mathbf{z}_x)$ and $q(\mathbf{z}_x|\mathbf{z}_t)$ are parameterized by the following:

$$q_{\mathbf{h}}(\mathbf{z}_x|\mathbf{z}_t) = C_q(\mathbf{z}_t) e^{(\mathbf{h}(\mathbf{z}_x)^T \mathbf{h}(\mathbf{z}_t)/\tau)}, \quad (19)$$

$$q_{\mathbf{h}}(\mathbf{z}_t|\mathbf{z}_x) = C_q(\mathbf{z}_x) e^{(\mathbf{h}(\mathbf{z}_t)^T \mathbf{h}(\mathbf{z}_x)/\tau)}, \quad (20)$$

with

$$C_q(\mathbf{z}_t) = \int e^{(\mathbf{h}(\mathbf{z}_x)^T \mathbf{h}(\mathbf{z}_t)/\tau)} d\mathbf{z}_x,$$

$$C_q(\mathbf{z}_x) = \int e^{(\mathbf{h}(\mathbf{z}_x)^T \mathbf{h}(\mathbf{z}_t)/\tau)} d\mathbf{z}_t.$$

To proof Theorem 3.1, we first introduce the following Lemma.

Lemma 4.1. *Consider the unit hypersphere space, given uniform prior $p(\mathbf{z}_x)$, $p(\mathbf{z}_x) = |\mathcal{Z}|^{-1}$ where $\mathcal{Z} \subseteq \mathbb{R}^M$ denotes the space of \mathbf{z}_x , and conditional distribution $p(\mathbf{z}_t|\mathbf{z}_x) = C_p(k) \exp(k\mathbf{z}_x^T \mathbf{z}_t)$, $p(\mathbf{z}_t)$ follows a uniform distribution.*

Proof. By Bayesian theorem, $p(\mathbf{z}_t) = \int p(\mathbf{z}_t|\mathbf{z}_x)p(\mathbf{z}_x)d\mathbf{z}_x = |\mathcal{Z}|^{-1} \int p(\mathbf{z}_t|\mathbf{z}_x)d\mathbf{z}_x = |\mathcal{Z}|^{-1} C_p(k) \int \exp(k\mathbf{z}_x^T \mathbf{z}_t)d\mathbf{z}_x$, then due to the unit hypersphere space, we have $\int \exp(k\mathbf{z}_x^T \mathbf{z}_t)d\mathbf{z}_x = C_p(k)^{-1}$. As a result, we obtain $p(\mathbf{z}_t) = |\mathcal{Z}|^{-1}$. \square

The proof of Theorem 3.1 relies on establishing the equality between the right-hand side of Eq. (18) and that of Eq. (14). Our initial step demonstrates that the global minimum of (14) necessitates $\mathbf{f}_x \circ \mathbf{g}_x = \mathbf{f}_t \circ \mathbf{g}_t$ for all real pairs $((\mathbf{m}_x, \mathbf{z}_x), (\mathbf{m}_t, \mathbf{z}_t))$. The second step involves demonstrating that the conditional distribution defined in (4), along with the aforementioned condition in the first step, guarantees two key properties: 1) $\mathbf{f}_x \circ \mathbf{g}_x = \mathbf{f}_t \circ \mathbf{g}_t$, and 2) their independence from the modality-specific variables \mathbf{m}_x and \mathbf{m}_t . Finally, by denoting $\mathbf{h} = \mathbf{f}_x \circ \mathbf{g}_x = \mathbf{f}_t \circ \mathbf{g}_t$ and applying the generative model defined in Eqs. (4)-(5) and the inference model outlined in Eqs (19)-(20), we arrive at the conclusion of the theorem.

Step I On hypersphere space, the d distance metric defined as cosine similarity in Eq. (14), thus we can rewrite the right-hand side of Eq. (14) as follows:

$$-2 \mathbb{E}_{(\mathbf{x}, \mathbf{t}) \sim p(\mathbf{x}, \mathbf{t})} [(\mathbf{f}_x(\mathbf{x})^T \mathbf{f}_t(\mathbf{t}))/\tau] + \mathbb{E}_{\mathbf{x} \sim p(\mathbf{x})} \left[\log \mathbb{E}_{\mathbf{t} \sim p(\mathbf{t})} [e^{(\mathbf{f}_x(\mathbf{x})^T \mathbf{f}_t(\mathbf{t}))/\tau}] \right] + \mathbb{E}_{\mathbf{t} \sim p(\mathbf{t})} \left[\log \mathbb{E}_{\mathbf{x} \sim p(\mathbf{x})} [e^{(\mathbf{f}_x(\mathbf{x})^T \mathbf{f}_t(\mathbf{t}))/\tau}] \right]. \quad (21)$$

Utilizing the generative model described in Eqs. (4)-(5), we can reframe Eq. (21) in terms of the latent variables $(\mathbf{m}_x, \mathbf{z}_x, \mathbf{m}_t, \mathbf{z}_t)$. Furthermore, by introducing the notations $\mathbf{h}_x = \mathbf{f}_x \circ \mathbf{g}_x$ and $\mathbf{h}_t = \mathbf{f}_t \circ \mathbf{g}_t$, we can express Eq. (21) as

follows:

$$\begin{aligned}
 & - 2 \mathbb{E}_{(\mathbf{m}_x, \mathbf{z}_x, \mathbf{m}_t, \mathbf{z}_t) \sim p(\mathbf{m}_x, \mathbf{z}_x, \mathbf{m}_t, \mathbf{z}_t)} \left[(\mathbf{h}_x(\mathbf{m}_x, \mathbf{z}_x)^T \mathbf{h}_t(\mathbf{m}_t, \mathbf{z}_t)) / \tau \right] \\
 & + \mathbb{E}_{(\mathbf{m}_x, \mathbf{z}_x) \sim p(\mathbf{m}_x, \mathbf{z}_x)} \left[\log \mathbb{E}_{(\mathbf{m}_t, \mathbf{z}_t) \sim p(\mathbf{m}_t, \mathbf{z}_t)} \left[e^{(\mathbf{h}_x(\mathbf{m}_x, \mathbf{z}_x)^T \mathbf{h}_t(\mathbf{m}_t, \mathbf{z}_t)) / \tau} \right] \right] \\
 & + \mathbb{E}_{(\mathbf{m}_t, \mathbf{z}_t) \sim p(\mathbf{m}_t, \mathbf{z}_t)} \left[\log \mathbb{E}_{(\mathbf{m}_x, \mathbf{z}_x) \sim p(\mathbf{m}_x, \mathbf{z}_x)} \left[e^{(\mathbf{h}_x(\mathbf{m}_x, \mathbf{z}_x)^T \mathbf{h}_t(\mathbf{m}_t, \mathbf{z}_t)) / \tau} \right] \right]. \tag{22}
 \end{aligned}$$

Further, since we assume the inference model as define in Eqs (19)-(20), and τ can be optimized in multimodal contrastive representation learning, we can further rewrite Eq. (22) as follows (see Appendix A.3 for details):

$$\begin{aligned}
 & - 2 \mathbb{E}_{(\mathbf{m}_x, \mathbf{z}_x, \mathbf{m}_t, \mathbf{z}_t) \sim p(\mathbf{m}_x, \mathbf{z}_x, \mathbf{m}_t, \mathbf{z}_t)} \left[(\mathbf{h}_x(\mathbf{m}_x, \mathbf{z}_x)^T \mathbf{h}_t(\mathbf{m}_t, \mathbf{z}_t)) / \tau \right] \\
 & - H(p(\mathbf{h}_x(\mathbf{m}_x, \mathbf{z}_x)), p(\mathbf{h}_t(\mathbf{m}_t, \mathbf{z}_t))) + \log Z_{\text{KDE}} \\
 & - H(p(\mathbf{h}_t(\mathbf{m}_t, \mathbf{z}_t)), p(\mathbf{h}_x(\mathbf{m}_x, \mathbf{z}_x))) + \log Z_{\text{KDE}}. \tag{23}
 \end{aligned}$$

This can be further formulated using the Kullback–Leibler divergence as follows:

$$- 2 \mathbb{E}_{(\mathbf{m}_x, \mathbf{z}_x, \mathbf{m}_t, \mathbf{z}_t) \sim p(\mathbf{m}_x, \mathbf{z}_x, \mathbf{m}_t, \mathbf{z}_t)} \left[(\mathbf{h}_x(\mathbf{m}_x, \mathbf{z}_x)^T \mathbf{h}_t(\mathbf{m}_t, \mathbf{z}_t)) / \tau \right] \tag{24}$$

$$- H(p(\mathbf{h}_x(\mathbf{m}_x, \mathbf{z}_x))) - D_{\text{KL}}(p(\mathbf{h}_x(\mathbf{m}_x, \mathbf{z}_x)) \| p(\mathbf{h}_t(\mathbf{m}_t, \mathbf{z}_t))) + \log Z_{\text{KDE}} \tag{25}$$

$$- H(p(\mathbf{h}_t(\mathbf{m}_t, \mathbf{z}_t))) - D_{\text{KL}}(p(\mathbf{h}_t(\mathbf{m}_t, \mathbf{z}_t)) \| p(\mathbf{h}_x(\mathbf{m}_x, \mathbf{z}_x))) + \log Z_{\text{KDE}}. \tag{26}$$

On hypersphere space with radius r , due to $\|\mathbf{h}_x(\mathbf{m}_x, \mathbf{z}_x) - \mathbf{h}_t(\mathbf{m}_t, \mathbf{z}_t)\| = 2r - 2\mathbf{h}_x(\mathbf{m}_x, \mathbf{z}_x)^T \mathbf{h}_t(\mathbf{m}_t, \mathbf{z}_t)$, the first term (24) is minimized if and only if

$$\mathbf{h}_x(\mathbf{m}_x, \mathbf{z}_x) = \mathbf{h}_t(\mathbf{m}_t, \mathbf{z}_t), \text{ holds for all real pairs } ((\mathbf{m}_x, \mathbf{z}_x), (\mathbf{m}_t, \mathbf{z}_t)). \quad (\text{condition 1}) \tag{27}$$

In addition, the last two terms, (25) and (26) is minimized if both \mathbf{h}_x and \mathbf{h}_t map $(\mathbf{m}_x, \mathbf{z}_x)$ and $(\mathbf{m}_t, \mathbf{z}_t)$, respectively, to uniform variables on hypersphere (condition 2, note that here uniform distributions also supports the symmetry of Eq. (19) and Eq. (20)). Since condition 1 does not affect the validity of condition 2, it follows that condition 1 is a necessary condition for minimizing the right-hand side of Eq. (18).

Step II By differentiating the equation with respect to \mathbf{m}_x in the condition 1 in the step I, we have:

$$\frac{\partial \mathbf{h}_x(\mathbf{m}_x, \mathbf{z}_x)}{\partial \mathbf{m}_x} = \frac{\partial \mathbf{h}_t(\mathbf{m}_t, \mathbf{z}_t)}{\partial \mathbf{m}_x} = 0, \tag{28}$$

, due to the independence between \mathbf{m}_x and $(\mathbf{m}_t, \mathbf{z}_t)$. Similarly, by differentiating the equation in the condition 1 with respect to \mathbf{m}_t , we have:

$$\frac{\partial \mathbf{h}_t(\mathbf{m}_t, \mathbf{z}_t)}{\partial \mathbf{m}_t} = \frac{\partial \mathbf{h}_x(\mathbf{m}_x, \mathbf{z}_x)}{\partial \mathbf{m}_t} = 0. \tag{29}$$

Based on Eqs. (28) and (29), we conclude that both \mathbf{h}_x and \mathbf{h}_t are independent of the modality-specific variables \mathbf{m}_x and \mathbf{m}_t , respectively, *i.e.*, $\mathbf{h}_x(\mathbf{m}_x, \mathbf{z}_x) = \mathbf{h}_x(\mathbf{z}_x)$ and $\mathbf{h}_t(\mathbf{m}_t, \mathbf{z}_t) = \mathbf{h}_t(\mathbf{z}_t)$. Further, since $\mathbf{h}_x(\mathbf{z}_x) = \mathbf{h}_t(\mathbf{z}_t)$ hold, for all real pairs $(\mathbf{z}_x, \mathbf{z}_t)$ sampled from the conditional distribution $p(\mathbf{z}_t | \mathbf{z}_x)$ defined in Eq. (4), this expression also holds true for $\mathbf{z}_t = \mathbf{z}_x$, which implies $\mathbf{h}_x(\mathbf{z}_x) = \mathbf{h}_t(\mathbf{z}_x)$. As a result, we can obtain: $\mathbf{h}_x = \mathbf{h}_t$.

Step III According to the results above: $\mathbf{h}_x(\mathbf{m}_x, \mathbf{z}_x) = \mathbf{h}_x(\mathbf{z}_x)$, $\mathbf{h}_t(\mathbf{m}_t, \mathbf{z}_t) = \mathbf{h}_t(\mathbf{z}_x)$, and $\mathbf{h}_x = \mathbf{h}_t$ from Step II, by defining $\mathbf{h} \stackrel{\text{def}}{=} \mathbf{h}_x = \mathbf{h}_t$, we can rewrite Eq. (21) as:

$$-2 \mathbb{E}_{(\mathbf{z}_x, \mathbf{z}_t) \sim p(\mathbf{z}_x, \mathbf{z}_t)} \left[(\mathbf{h}(\mathbf{z}_x)^T \mathbf{h}(\mathbf{z}_t)) / \tau \right] + \mathbb{E}_{\mathbf{z}_x \sim p(\mathbf{z}_x)} \left[\log \mathbb{E}_{\mathbf{z}_t \sim p(\mathbf{z}_t)} \left[e^{(\mathbf{h}(\mathbf{z}_x)^T \mathbf{h}(\mathbf{z}_t)) / \tau} \right] \right] + \mathbb{E}_{\mathbf{z}_t \sim p(\mathbf{z}_t)} \left[\log \mathbb{E}_{\mathbf{z}_x \sim p(\mathbf{z}_x)} \left[e^{(\mathbf{h}(\mathbf{z}_x)^T \mathbf{h}(\mathbf{z}_t)) / \tau} \right] \right]. \tag{30}$$

We then connect the right-hand side of Eq. (18) with Eq. (30). To this end, since the two terms in the right-hand side of Eq. (18) are symmetrical, we focus on one of the two terms for convenience, *e.g.*, $\mathbb{E}_{\mathbf{z}_x \sim p(\mathbf{z}_x)} [H(p(\mathbf{z}_t|\mathbf{z}_x)), q_{\mathbf{h}}(\mathbf{z}_t|\mathbf{z}_x)]$. Based on Lemma 4.1, it can be shown that:

$$\mathbb{E}_{\mathbf{z}_x \sim p(\mathbf{z}_x)} [H(p(\mathbf{z}_t|\mathbf{z}_x)), q_{\mathbf{h}}(\mathbf{z}_t|\mathbf{z}_x)] \quad (31)$$

$$\mathbb{E}_{\mathbf{z}_x \sim p(\mathbf{z}_x)} \left[\mathbb{E}_{\mathbf{z}_t \sim p(\mathbf{z}_t|\mathbf{z}_x)} [-\log q_{\mathbf{h}}(\mathbf{z}_t|\mathbf{z}_x)] \right] \quad (32)$$

$$= - \mathbb{E}_{(\mathbf{z}_x, \mathbf{z}_t) \sim p(\mathbf{z}_x, \mathbf{z}_t)} \left[-\mathbf{h}(\mathbf{z}_x)^T \mathbf{h}(\mathbf{z}_t) / \tau + \log C_q(\mathbf{z}_x) \right] \quad (33)$$

$$= \mathbb{E}_{(\mathbf{z}_x, \mathbf{z}_t) \sim p(\mathbf{z}_x, \mathbf{z}_t)} \left[-\mathbf{h}(\mathbf{z}_x)^T \mathbf{h}(\mathbf{z}_t) / \tau \right] + \mathbb{E}_{(\mathbf{z}_x) \sim p(\mathbf{z}_x)} [\log C_q(\mathbf{z}_x)] \quad (34)$$

$$= \mathbb{E}_{(\mathbf{z}_x, \mathbf{z}_t) \sim p(\mathbf{z}_x, \mathbf{z}_t)} \left[-\mathbf{h}(\mathbf{z}_x)^T \mathbf{h}(\mathbf{z}_t) / \tau \right] + \mathbb{E}_{(\mathbf{z}_x) \sim p(\mathbf{z}_x)} \left[\log \int e^{(\mathbf{h}(\mathbf{z}_x)^T \mathbf{h}(\mathbf{z}_t) / \tau)} d\mathbf{z}_x \right] \quad (35)$$

Since $p(\mathbf{z}_x) = |\mathcal{Z}|^{-1}$, and $p(\mathbf{z}_t) = |\mathcal{Z}|^{-1}$ by Lemma 4.1, Eq. (35) is equal to:

$$= - \mathbb{E}_{(\mathbf{z}_x, \mathbf{z}_t) \sim p(\mathbf{z}_x, \mathbf{z}_t)} \left[(\mathbf{h}(\mathbf{z}_x)^T \mathbf{h}(\mathbf{z}_t)) / \tau \right] + \mathbb{E}_{\mathbf{z}_x \sim p(\mathbf{z}_x)} \left[\log \mathbb{E}_{\mathbf{z}_t \sim p(\mathbf{z}_t)} \left[e^{(\mathbf{h}(\mathbf{z}_x)^T \mathbf{h}(\mathbf{z}_t) / \tau)} \right] \right] \quad (36)$$

Similarly, for the second term in the right-hand side of Eq. (18), we can proof that:

$$\mathbb{E}_{(\mathbf{z}_t) \sim p(\mathbf{z}_t)} [H(p(\mathbf{z}_x|\mathbf{z}_t)), q_{\mathbf{h}}(\mathbf{z}_x|\mathbf{z}_t)] = - \mathbb{E}_{(\mathbf{z}_x, \mathbf{z}_t) \sim p(\mathbf{z}_x, \mathbf{z}_t)} \left[(\mathbf{h}(\mathbf{z}_x)^T \mathbf{h}(\mathbf{z}_t)) / \tau \right] + \mathbb{E}_{\mathbf{z}_t \sim p(\mathbf{z}_t)} \left[\log \mathbb{E}_{\mathbf{z}_x \sim p(\mathbf{z}_x)} \left[e^{(\mathbf{h}(\mathbf{z}_x)^T \mathbf{h}(\mathbf{z}_t) / \tau)} \right] \right]. \quad (37)$$

By combining Eq. (36) and Eq. (37), we can conclude the proof.

A.4.2. IDENTIFIABILITY RESULT ON HYPERSPHERE

Theorem 3.1 represents a adaptation of Theorem 1 from Zimmermann et al. (2021) in the context of multi-modal setting. Specifically, within the confines of a single-modal framework, Theorem 3.1 is consistent with the findings presented in Theorem 1 in Zimmermann et al. (2021). Consequently, this alignment allows us to employ Propositions 1 and 2 from Zimmermann et al. (2021) to demonstrate that the global minimization of the objective outlined in Equation (6), as specified in Theorem 3.1, identifies the latent variables \mathbf{z}_x , as well as \mathbf{z}_x , up to linear transformations. For completeness, a brief proof is provided herein, with comprehensive details available in the original work. Clearly, the global minimum of the cross-entropy between two distributions is reached if they match by value and have the same support. Therefore, for the optimal solution of the objective loss Eq. (18) in Theorem 3.1, we have:

$$p(\mathbf{z}_t|\mathbf{z}_x) = q_{\mathbf{h}}(\mathbf{z}_t|\mathbf{z}_x), \quad (38)$$

This expression also holds true for $\mathbf{z}_t = \mathbf{z}_x$; additionally using that \mathbf{h} maps from a unit hypersphere to one with radius $\sqrt{\tau k}$, we have:

$$\begin{aligned} C_p e^{(k\mathbf{z}_x^T \mathbf{z}_x)} &= C_q(\mathbf{z}_x) e^{(\mathbf{h}(\mathbf{z}_x)^T \mathbf{h}(\mathbf{z}_x) / \tau)}, \\ \Leftrightarrow C_p &= C_q(\mathbf{z}_x) \end{aligned} \quad (39)$$

As the normalization constants are identical we get for all $\mathbf{z}_x, \mathbf{z}_t$,

$$k\mathbf{z}_x^T \mathbf{z}_t = \mathbf{h}(\mathbf{z}_x)^T \mathbf{h}(\mathbf{z}_t) / \tau, \quad (40)$$

here we can see that \mathbf{h} maintains the dot product, which implies that \mathbf{h} must be an orthogonal linear transformation by using Proposition 2 in Zimmermann et al. (2021). As a result, Theorem 3.1 is capable of identifying the latent variables \mathbf{z}_x and \mathbf{z}_t up to an orthogonal linear transformation, *i.e.*, the recovered latent variable $\hat{\mathbf{z}}_x$, obtained through the minimization of Equation (6), is linearly related to the true \mathbf{z}_x as follows: $\hat{\mathbf{z}}_x = \mathbf{A}\mathbf{z}_x + \mathbf{c}$, where \mathbf{A} represents an orthogonal matrix, and \mathbf{c} is a constant vector.

A.5. The Proof of identifiability on convex bodies

A.5.1. THE PROOF OF THEOREM 3.2

Theorem 3.2. (*\mathcal{L} converges to the symmetric cross-entropy*) Under the assumptions defined in Eqs. (9)-(10) for the proposed latent partial causal model, the necessary condition $\mathbf{f}_x \circ \mathbf{g}_x = \mathbf{f}_t \circ \mathbf{g}_t$, denoted as \mathbf{h} , for the optimal normalized symmetric contrastive loss given by Eq. (2) leads to the following reduction of the loss itself:

$$\lim_{N \rightarrow \infty} \mathcal{L} - 2 \log N = \mathbb{E}_{\mathbf{z}_x \sim p(\mathbf{z}_x)} [H(p(\mathbf{z}_t|\mathbf{z}_x)), q_{\mathbf{h}}(\mathbf{z}_t|\mathbf{z}_x)] + \mathbb{E}_{(\mathbf{z}_t) \sim p(\mathbf{z}_t)} [H(p(\mathbf{z}_x|\mathbf{z}_t)), q_{\mathbf{h}}(\mathbf{z}_x|\mathbf{z}_t)] \quad (41)$$

where H is the cross entropy, the conditional distributions $q_{\mathbf{h}}(\mathbf{z}_t|\mathbf{z}_x)$ and $q(\mathbf{z}_x|\mathbf{z}_t)$ are parameterized by the following:

$$q_{\mathbf{h}}(\mathbf{z}_x|\mathbf{z}_t) = C_q(\mathbf{z}_t) e^{-\delta(\mathbf{h}(\mathbf{z}_x), \mathbf{h}(\mathbf{z}_t))/\tau}, \quad (42)$$

$$q_{\mathbf{h}}(\mathbf{z}_t|\mathbf{z}_x) = C_q(\mathbf{z}_x) e^{-\delta(\mathbf{h}(\mathbf{z}_x), \mathbf{h}(\mathbf{z}_t))/\tau}, \quad (43)$$

with

$$C_q(\mathbf{z}_t) = \int e^{-\delta(\mathbf{h}(\mathbf{z}_x), \mathbf{h}(\mathbf{z}_t))/\tau} d\mathbf{z}_x,$$

$$C_q(\mathbf{z}_x) = \int e^{-\delta(\mathbf{h}(\mathbf{z}_x), \mathbf{h}(\mathbf{z}_t))/\tau} d\mathbf{z}_t.$$

Similar to the proof A.4.1, we first introduce the following Lemma.

Lemma 4.2. For random variables $\mathbf{z}_x \in \mathcal{Z}_c$ and $\mathbf{z}_t \in \mathcal{Z}_c$, assume that $p(\mathbf{z}_x) = 1/|\mathcal{Z}_c|$ if $\mathbf{z}_x \in \mathcal{Z}_c$ and 0 otherwise, and assume that conditional distribution $p(\mathbf{z}_t|\mathbf{z}_x) = C(\mathbf{z}_x) \exp(-\delta(\mathbf{z}_x, \mathbf{z}_t)/\lambda)$, where δ is a symmetric metric induced by a norm, then $p(\mathbf{z}_t)$ converges to uniform distribution on \mathcal{Z}_c as $\lambda \rightarrow 0_+$.

Proof. The proof can be done by the fact that as $\lambda \rightarrow 0$, the condition distribution $p(\mathbf{z}_t|\mathbf{z}_x)$ converges to a delta distribution, resulting that $p(\mathbf{z}_t) = p(\mathbf{z}_x)$. More specifically, as we will let $\lambda \rightarrow 0$ in the procedure, it is notable that the normalize $C(\mathbf{z}_x)$ actually depend on λ and should be write as $C(\mathbf{z}_x, \lambda)$ in a more formal way. With simple integration trick, it would be straightforward to show that $C(\mathbf{z}_x, \lambda)$ can be decomposed as $C(\mathbf{z}_x, \lambda) = \frac{1}{\lambda} C'(\mathbf{z}_x)$.

By definition we have

$$\begin{aligned} p(\mathbf{z}_t) &= \int_{\mathbf{z}_x \in \mathcal{Z}_c} p(\mathbf{z}_x) p(\mathbf{z}_t|\mathbf{z}_x) d\mathbf{z}_x \\ &= \int_{\mathbf{z}_x \in \mathcal{Z}_c} p(\mathbf{z}_x) \frac{1}{\lambda} C'(\mathbf{z}_x) \exp(-\delta(\mathbf{z}_x, \mathbf{z}_t)/\lambda) d\mathbf{z}_x \\ &= \lim_{N \rightarrow +\infty} \sum_{i=1}^N \frac{1}{\lambda} C'(\mathbf{z}_{x_i}) \exp(-\delta(\mathbf{z}_{x_i}, \mathbf{z}_t)/\lambda), \forall i, \mathbf{z}_{x_i} \sim p(\mathbf{z}_x) \end{aligned} \quad (44)$$

then obviously we have that

$$\begin{aligned} \lim_{\lambda \rightarrow 0_+} p(\mathbf{z}_t) &= \lim_{\lambda \rightarrow 0_+} \lim_{N \rightarrow +\infty} \sum_{i=1}^N \frac{1}{\lambda} C'(\mathbf{z}_{x_i}) \exp(-\delta(\mathbf{z}_{x_i}, \mathbf{z}_t)/\lambda) \\ &= \lim_{\lambda \rightarrow 0_+} \lim_{N \rightarrow +\infty} \sum_{i=1}^N \frac{1}{\lambda} C' \exp(-\delta(\mathbf{z}_{x_i}, \mathbf{z}_t)/\lambda), \end{aligned} \quad (45)$$

where $C' = \int_{-\infty}^{\infty} \exp(-\delta(\mathbf{0}, \mathbf{z}_t)) d\mathbf{z}_t$. It is obvious that (45) can be viewed as a Kernel Density Estimation over samples $\mathbf{z}_{x_i} \sim p(\mathbf{z}_x)$, and obviously $\lim_{\tau \rightarrow 0_+} p(\mathbf{z}_t)$ will converge to $p(\mathbf{z}_x)$ (which is uniform distribution) under quite mild condition (for details of the convergence we refer to (Jiang, 2017)). \square

The proof of Theorem 3.2 can be done by demonstrating that the right-hand side of Eq. (41) is equal to the right-hand side of Eq. (14) on convex bodies. To achieve this, we first demonstrate that the minimization of (14) implies that the following condition hold: $\mathbf{f}_x \circ \mathbf{g}_x(\mathbf{m}_x, \mathbf{z}_x) = \mathbf{f}_t \circ \mathbf{g}_t(\mathbf{m}_t, \mathbf{z}_t)$, for all real pairs $((\mathbf{m}_x, \mathbf{z}_x), (\mathbf{m}_t, \mathbf{z}_t))$. In the second step, by the condition above, we show that $\mathbf{f}_x \circ \mathbf{g}_x = \mathbf{f}_t \circ \mathbf{g}_t$, and they are independent of the modality-specific variables \mathbf{m}_x and \mathbf{m}_t , respectively. Finally, by defining $\mathbf{h} = \mathbf{f}_x \circ \mathbf{g}_x = \mathbf{f}_t \circ \mathbf{g}_t$, and using the inference model (42) and (43), we obtain our result.

Step I On convex bodies, similar to Eqs. (21)-(26), and define $\mathbf{h}_x = \mathbf{f}_x \circ \mathbf{g}_x$ and $\mathbf{h}_t = \mathbf{f}_t \circ \mathbf{g}_t$, we can further rewrite the right-hand side of Eq. (14) as:

$$-2 \mathbb{E}_{(\mathbf{m}_x, \mathbf{z}_x, \mathbf{m}_t, \mathbf{z}_t) \sim p(\mathbf{m}_x, \mathbf{z}_x, \mathbf{m}_t, \mathbf{z}_t)} [d(\mathbf{h}_x(\mathbf{m}_x, \mathbf{z}_x), \mathbf{h}_t(\mathbf{m}_t, \mathbf{z}_t)) / \tau] \quad (46)$$

$$- H(p(\mathbf{h}_x(\mathbf{m}_x, \mathbf{z}_x))) - D_{\text{KL}}(p(\mathbf{h}_x(\mathbf{m}_x, \mathbf{z}_x)) \| p(\mathbf{h}_t(\mathbf{m}_t, \mathbf{z}_t))) + \log Z_{\text{KDE}} \quad (47)$$

$$- H(p(\mathbf{h}_t(\mathbf{m}_t, \mathbf{z}_t))) - D_{\text{KL}}(p(\mathbf{h}_t(\mathbf{m}_t, \mathbf{z}_t)) \| p(\mathbf{h}_x(\mathbf{m}_x, \mathbf{z}_x))) + \log Z_{\text{KDE}}. \quad (48)$$

Again, on convex bodies, since d denote a distance metric, the first term (46) is minimized if and only if

$$\mathbf{h}_x(\mathbf{m}_x, \mathbf{z}_x) = \mathbf{h}_t(\mathbf{m}_t, \mathbf{z}_t), \text{ holds for all real pairs } ((\mathbf{m}_x, \mathbf{z}_x), (\mathbf{m}_t, \mathbf{z}_t)). \quad (\text{condition 1\#}) \quad (49)$$

In addition, the last two terms, (47) and (48) is minimized if both \mathbf{h}_x and \mathbf{h}_t map $(\mathbf{m}_x, \mathbf{z}_x)$ and $(\mathbf{m}_t, \mathbf{z}_t)$, respectively, to uniform variables on hypersphere (condition 2#, note that here uniform distributions also supports the symmetry of Eq. (42) and Eq. (43)). Since condition 1# does not affect the validity of condition 2#, it follows that condition 1# is a necessary condition for minimizing the right-hand side of Eq. (18).

Step II Similar to Step II in Appendix A.4.1, by differentiating the equation in the condition 1# with respect to \mathbf{m}_x and \mathbf{m}_t , respectively, we can conclude that both \mathbf{h}_x and \mathbf{h}_t are independent of the modality-specific variables \mathbf{m}_x and \mathbf{m}_t , respectively, *i.e.*, $\mathbf{h}_x(\mathbf{m}_x, \mathbf{z}_x) = \mathbf{h}_x(\mathbf{z}_x)$ and $\mathbf{h}_t(\mathbf{m}_t, \mathbf{z}_t) = \mathbf{h}_t(\mathbf{z}_t)$. Further, since $\mathbf{h}_x(\mathbf{z}_x) = \mathbf{h}_t(\mathbf{z}_t)$ hold, for all real pairs $(\mathbf{z}_x, \mathbf{z}_t)$ sampled from the conditional distribution $p(\mathbf{z}_t | \mathbf{z}_x)$ defined in Eq. (9), this expression also holds true for $\mathbf{z}_t = \mathbf{z}_x$, which implies $\mathbf{h}_x(\mathbf{z}_x) = \mathbf{h}_t(\mathbf{z}_x)$. As a result, we can obtain: $\mathbf{h}_x = \mathbf{h}_t$.

Step III According to the results above: $\mathbf{h}_x(\mathbf{m}_x, \mathbf{z}_x) = \mathbf{h}_x(\mathbf{z}_x)$, $\mathbf{h}_t(\mathbf{m}_t, \mathbf{z}_t) = \mathbf{h}_t(\mathbf{z}_t)$, and $\mathbf{h}_x = \mathbf{h}_t$, by defining $\mathbf{h} \stackrel{\text{def}}{=} \mathbf{f}_x \circ \mathbf{g}_x = \mathbf{f}_t \circ \mathbf{g}_t$, we can rewrite Eq. (21) as:

$$-2 \mathbb{E}_{(\mathbf{z}_x, \mathbf{z}_t) \sim p(\mathbf{z}_x, \mathbf{z}_t)} [d(\mathbf{h}(\mathbf{z}_x), \mathbf{h}(\mathbf{z}_t)) / \tau] + \mathbb{E}_{\mathbf{z}_x \sim p(\mathbf{z}_x)} \left[\log \mathbb{E}_{\mathbf{z}_t \sim p(\mathbf{z}_t)} [e^{d(\mathbf{h}(\mathbf{z}_x), \mathbf{h}(\mathbf{z}_t)) / \tau}] \right] + \mathbb{E}_{\mathbf{z}_t \sim p(\mathbf{z}_t)} \left[\log \mathbb{E}_{\mathbf{z}_x \sim p(\mathbf{z}_x)} [e^{d(\mathbf{h}(\mathbf{z}_x), \mathbf{h}(\mathbf{z}_t)) / \tau}] \right]. \quad (50)$$

We then connect the right-hand side of Eq. (41) with Eq. (50). To this end, since the two terms in the right-hand side of Eq. (41) are symmetrical, we focus on one of the two terms for convenience, *e.g.*, $\mathbb{E}_{\mathbf{z}_x \sim p(\mathbf{z}_x)} [H(p(\mathbf{z}_t | \mathbf{z}_x)), q_{\mathbf{h}}(\mathbf{z}_t | \mathbf{z}_x)]$. It can be shown that:

$$\mathbb{E}_{\mathbf{z}_x \sim p(\mathbf{z}_x)} [H(p(\mathbf{z}_t | \mathbf{z}_x)), q_{\mathbf{h}}(\mathbf{z}_t | \mathbf{z}_x)] \quad (51)$$

$$\mathbb{E}_{\mathbf{z}_x \sim p(\mathbf{z}_x)} \left[\mathbb{E}_{\mathbf{z}_t \sim p(\mathbf{z}_t | \mathbf{z}_x)} [-\log q_{\mathbf{h}}(\mathbf{z}_t | \mathbf{z}_x)] \right] \quad (52)$$

$$= - \mathbb{E}_{(\mathbf{z}_x, \mathbf{z}_t) \sim p(\mathbf{z}_x, \mathbf{z}_t)} [-d(\mathbf{h}(\mathbf{z}_x), \mathbf{h}(\mathbf{z}_t)) / \tau + \log C_q(\mathbf{z}_x)] \quad (53)$$

$$= \mathbb{E}_{(\mathbf{z}_x, \mathbf{z}_t) \sim p(\mathbf{z}_x, \mathbf{z}_t)} [-d(\mathbf{h}(\mathbf{z}_x), \mathbf{h}(\mathbf{z}_t)) / \tau] + \mathbb{E}_{(\mathbf{z}_x) \sim p(\mathbf{z}_x)} [\log C_q(\mathbf{z}_x)] \quad (54)$$

$$= \mathbb{E}_{(\mathbf{z}_x, \mathbf{z}_t) \sim p(\mathbf{z}_x, \mathbf{z}_t)} [-d(\mathbf{h}(\mathbf{z}_x), \mathbf{h}(\mathbf{z}_t)) / \tau] + \mathbb{E}_{(\mathbf{z}_x) \sim p(\mathbf{z}_x)} \left[\log \int e^{(d(\mathbf{h}(\mathbf{z}_x), \mathbf{h}(\mathbf{z}_t)) / \tau)} d\mathbf{z}_x \right] \quad (55)$$

Since $p(\mathbf{z}_x) = |\mathcal{Z}|^{-1}$, and $p(\mathbf{z}_t) = |\mathcal{Z}|^{-1}$ by Lemma 4.2, Eq. (55) is equal to:

$$= - \mathbb{E}_{(\mathbf{z}_x, \mathbf{z}_t) \sim p(\mathbf{z}_x, \mathbf{z}_t)} [d(\mathbf{h}(\mathbf{z}_x), \mathbf{h}(\mathbf{z}_t)) / \tau] + \mathbb{E}_{\mathbf{z}_x \sim p(\mathbf{z}_x)} \left[\log \mathbb{E}_{\mathbf{z}_t \sim p(\mathbf{z}_t)} [e^{d(\mathbf{h}(\mathbf{z}_x), \mathbf{h}(\mathbf{z}_t)) / \tau}] \right] \quad (56)$$

Similarly, for the second term in the right-hand side of Eq. (41), we can proof that:

$$\mathbb{E}_{(\mathbf{z}_t) \sim p(\mathbf{z}_t)} [H(p(\mathbf{z}_x|\mathbf{z}_t)), q_{\mathbf{h}}(\mathbf{z}_x|\mathbf{z}_t))] = - \mathbb{E}_{(\mathbf{z}_x, \mathbf{z}_t) \sim p(\mathbf{z}_x, \mathbf{z}_t)} [d(\mathbf{h}(\mathbf{z}_x), \mathbf{h}(\mathbf{z}_t))/\tau] + \mathbb{E}_{\mathbf{z}_t \sim p(\mathbf{z}_t)} \left[\log \mathbb{E}_{\mathbf{z}_x \sim p(\mathbf{z}_x)} [e^{d(\mathbf{h}(\mathbf{z}_x), \mathbf{h}(\mathbf{z}_t))/\tau}] \right]. \quad (57)$$

By combining Eq. (56) and Eq. (57), we can conclude the proof.

A.5.2. IDENTIFIABILITY RESULT ON CONVEX BODIES

Theorem 3.2 represents a symmetrical adaptation of Theorem 3 from Zimmermann et al. (2021). This alignment allows us to employ Propositions 4, Lemma 1 and Lemma A from Zimmermann et al. (2021) to demonstrate that the global minimization of the objective outlined in Equation (41), as specified in Theorem 3.2, identifies the latent variables \mathbf{z}_x , as well as \mathbf{z}_t , up to linear transformations. For completeness, a brief proof is provided herein, with comprehensive details available in the original work. Clearly, the global minimum of the cross-entropy between two distributions is reached if they match by value and have the same support. Therefore, for the optimal solution of the objective loss Eq. (14) in Theorem 3.2, we have:

$$p(\mathbf{z}_t|\mathbf{z}_x) = q_{\mathbf{h}}(\mathbf{z}_t|\mathbf{z}_x), \quad (58)$$

This expression also holds true for $\mathbf{z}_t = \mathbf{z}_x$, we have:

$$\begin{aligned} C_p(\mathbf{z}_x) e^{-\delta(\mathbf{z}_x, \mathbf{z}_x)/\lambda} &= C_q(\mathbf{z}_x) e^{-\delta(\mathbf{h}(\mathbf{z}_x), \mathbf{h}(\mathbf{z}_x))/\tau}, \\ \Leftrightarrow C_p(\mathbf{z}_x) &= C_q(\mathbf{z}_x) \end{aligned} \quad (59)$$

As the normalization constants are identical we get for all $\mathbf{z}_x, \mathbf{z}_t$,

$$\delta(\mathbf{z}_x, \mathbf{z}_t) = \lambda \delta(\mathbf{h}(\mathbf{z}_x), \mathbf{h}(\mathbf{z}_t))/\tau. \quad (60)$$

Then, by limiting δ be an L^α metric for $\alpha \geq 1$, $\alpha \neq 2$ or the α -th power of such an L^α metric, using the Theorem 5 in Zimmermann et al. (2021), Theorem 3.1 can identify the latent variables \mathbf{z}_x and \mathbf{z}_t up to an permutation transformation, *i.e.*, the recovered latent variable $\hat{\mathbf{z}}_x$, obtained through the minimization of Equation (11), is related to the true \mathbf{z}_x as follows: $\hat{\mathbf{z}}_x = \mathbf{P}\mathbf{z}_x + \mathbf{c}$, where \mathbf{P} represents an permutation matrix with scaling, and \mathbf{c} is a constant vector.

A.6. More Results on CelebA

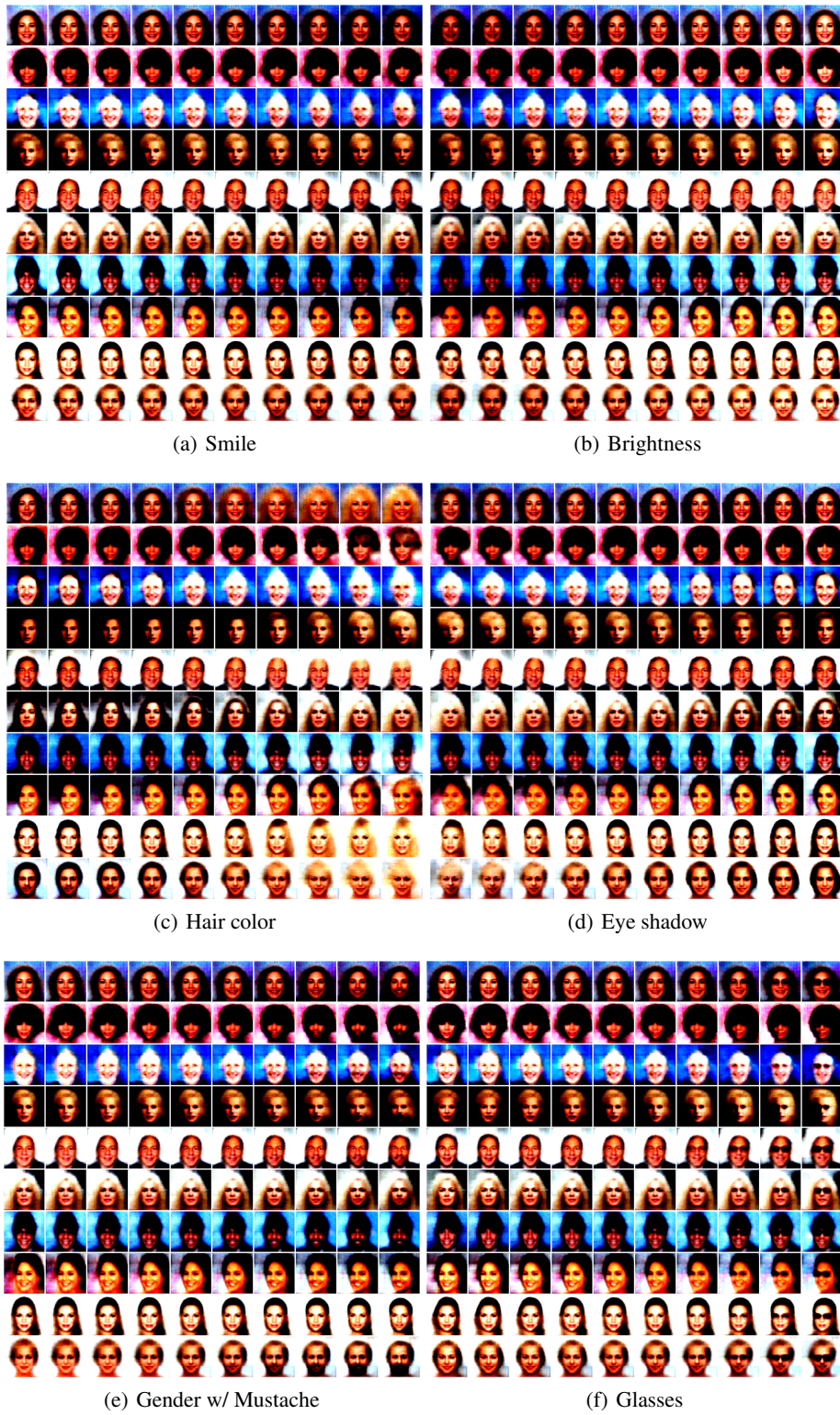


Figure 3. Disentangled Representations learned by combining pre-train CLIP and FastICA.

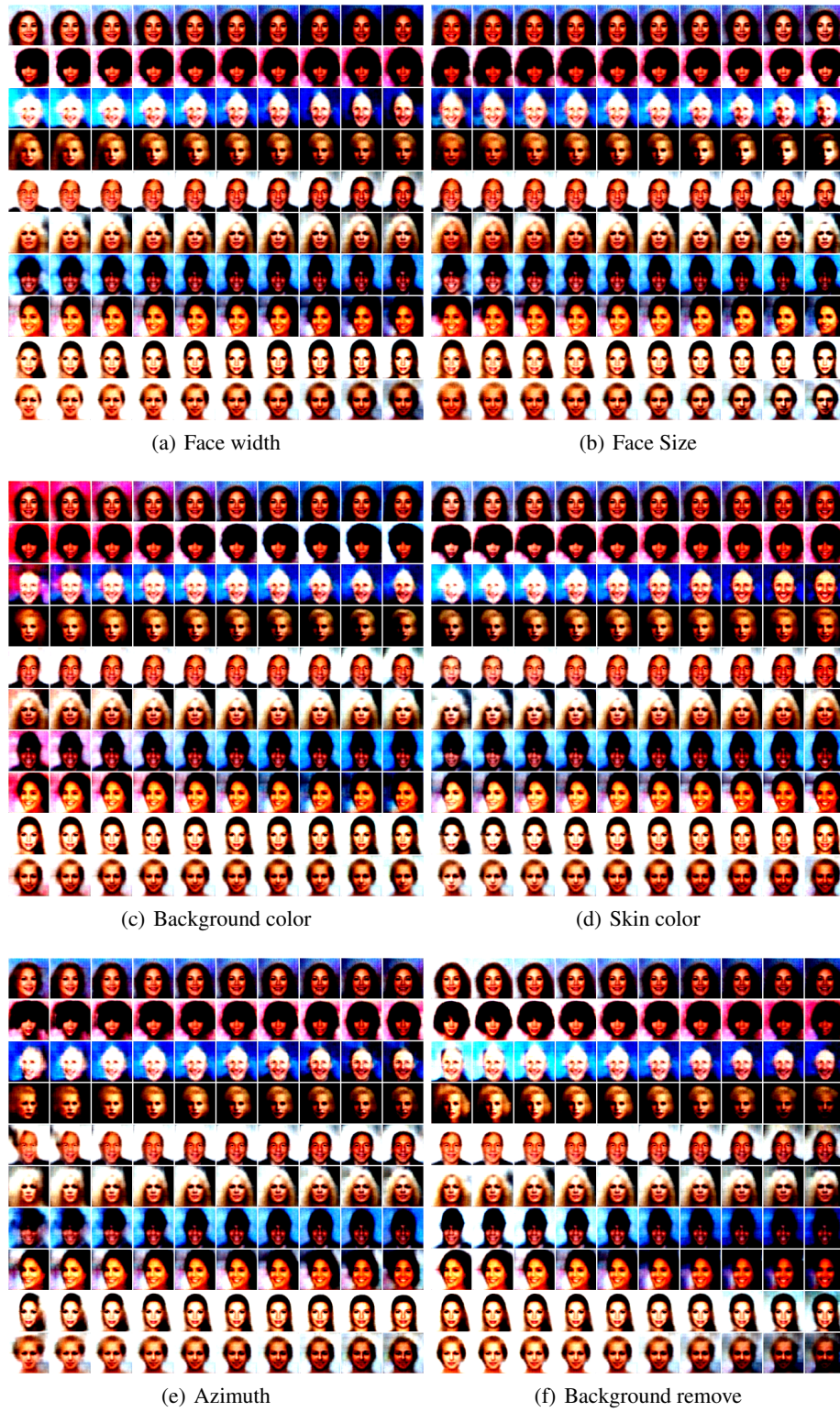


Figure 4. Disentangled Representations learned by combining pre-train CLIP and FastICA.

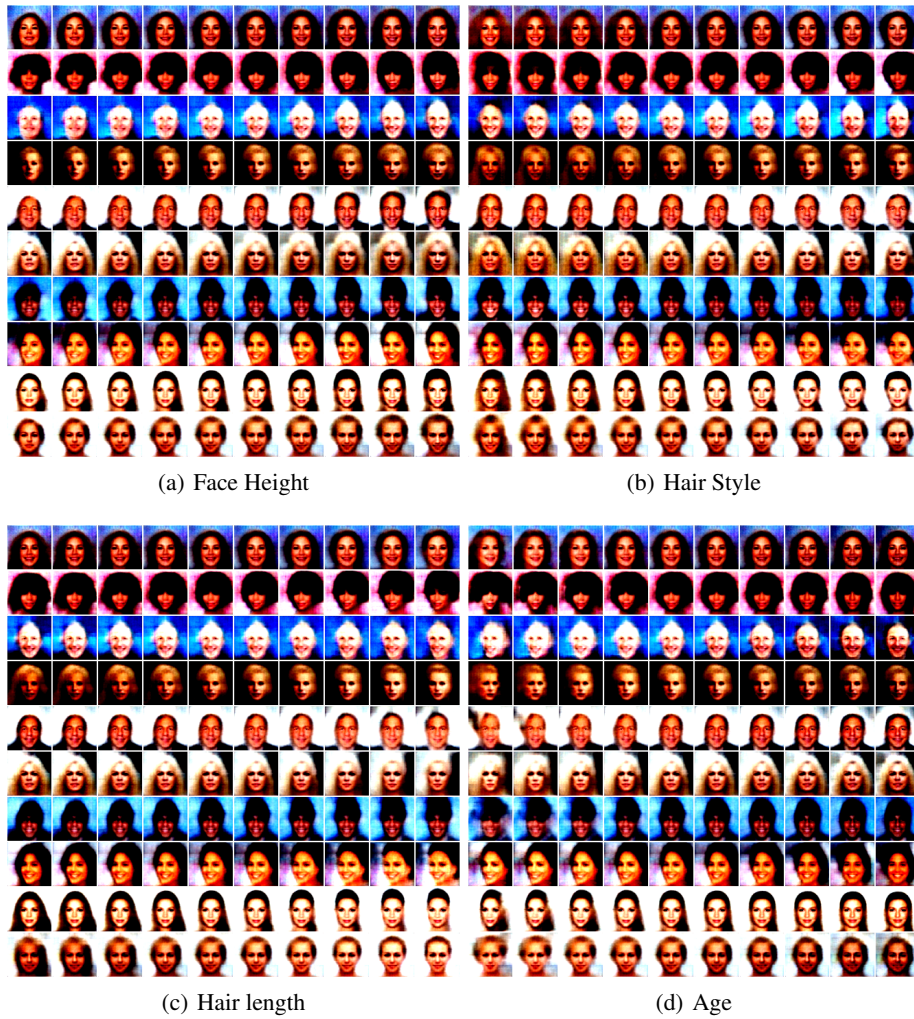


Figure 5. Disentangled Representations learned by combining pre-train CLIP and FastICA.

A.7. More Results on ImageNet-Type Data

Table 5. Quantitative results for 16-shot transfer learning and domain generalization by different methods. Lin. P. (Linear Probe).

ENCODERS	METHODS	SOURCE		TARGET (IMAGENET-)			
		IMAGENET	V2	SKETCH	R	A	AVG.
RN50	LIN. P.	55.36	45.45	18.22	34.09	12.52	27.77
	LIN. P. w/ FASTICA	57.82	47.78	19.77	38.05	13.15	29.69
	LIN. P. w/ PCA AND FASTICA	57.37	47.67	20.39	38.76	12.89	29.93
RN101	LIN. P.	60.98	50.36	25.80	46.61	18.64	35.35
	LIN. P. w/ FASTICA	61.86	51.85	27.29	49.29	19.89	37.08
	LIN. P. w/ PCA AND FASTICA	61.58	51.44	28.86	50.32	19.97	37.64
ViT32	LIN. P.	60.76	50.92	28.81	49.18	19.72	37.15
	LIN. P. w/ FASTICA	61.94	51.95	30.30	51.82	20.81	38.72
	LIN. P. w/ PCA AND FASTICA	62.00	52.39	30.39	51.61	20.96	38.84
ViT16	LIN. P.	67.17	57.01	35.43	60.96	35.41	47.20
	LIN. P. w/ PCA AND FASTICA	68.12	58.45	38.41	63.89	37.17	49.48
	LIN. P. w/ FASTICA	67.96	58.38	38.75	65.45	38.28	50.22

Table 6. Quantitative results for 8-shot transfer learning and domain generalization by different methods. Lin. P. (Linear Probe).

ENCODERS	METHODS	SOURCE		TARGET (IMAGENET-)			
		IMAGENET	V2	SKETCH	R	A	AVG.
RN50	LIN. P.	49.33	40.83	15.06	31.23	10.99	24.53
	LIN. P. w/ FASTICA	51.99	43.58	15.47	34.35	12.85	26.56
	LIN. P. w/ PCA AND FASTICA	51.42	42.93	17.28	35.53	12.33	27.02
RN101	LIN. P.	55.41	46.04	23.38	43.26	16.88	32.39
	LIN. P. w/ FASTICA	56.59	47.47	22.09	44.59	18.39	33.14
	LIN. P. w/ PCA AND FASTICA	55.84	46.59	23.68	44.94	18.25	33.37
ViT32	LIN. P.	55.17	46.11	25.53	45.32	18.35	33.83
	LIN. P. w/ FASTICA	56.90	47.96	27.62	49.13	20.31	36.26
	LIN. P. w/ PCA AND FASTICA	55.83	46.55	26.54	46.77	18.80	34.67
ViT16	LIN. P.	61.82	52.34	32.26	55.93	32.63	43.29
	LIN. P. w/ FASTICA	63.55	54.81	34.21	61.54	38.21	47.29
	LIN. P. w/ PCA AND FASTICA	63.47	54.32	35.83	61.88	37.35	47.36

Table 7. Quantitative results for 1-shot transfer learning and domain generalization by different methods. Lin. P. (Linear Probe).

ENCODERS	METHODS	SOURCE		TARGET (IMAGENET-)			
		IMAGENET	V2	SKETCH	R	A	AVG.
RN50	LIN. P.	21.74	18.24	5.68	15.41	6.55	11.47
	LIN. P. W/ FASTICA	23.22	19.68	6.37	13.84	7.21	11.77
	LIN. P. W/ FASTICA	24.06	20.26	6.85	17.54	8.05	13.18
RN101	LIN. P.	26.05	21.48	9.90	23.85	10.17	16.35
	LIN. P. W/ FASTICA	27.50	23.33	8.35	17.87	10.71	15.07
	LIN. P. W/ PCA AND FASTICA	28.50	24.17	11.63	26.38	12.28	18.62
ViT32	LIN. P.	26.99	22.99	11.93	25.25	11.56	17.93
	LIN. P. W/ FASTICA	29.21	24.80	9.97	21.23	12.23	17.06
	LIN. P. W/ PCA AND FASTICA	29.05	24.45	12.39	27.61	12.56	19.25
ViT16	LIN. P.	32.42	27.64	16.34	34.28	21.84	25.02
	LIN. P. W/ FASTICA	34.35	29.31	13.91	28.61	23.24	23.77
	LIN. P. W/ PCA AND FASTICA	35.20	30.26	19.17	38.87	26.41	28.68

ReLU(BN(ConvTranspose2d(512, 512, kernelsize=1, stride=1, padding=0)))
ReLU(BN(ConvTranspose2d(512, 64, kernelsize=4, stride=1, padding=0)))
ReLU(BN(ConvTranspose2d(64, 64, kernelsize=4, stride=1, padding=0)))
ReLU(BN(ConvTranspose2d(64, 32, kernelsize=4, stride=1, padding=0)))
ReLU(BN(ConvTranspose2d(32, 32, kernelsize=4, stride=1, padding=0)))
ConvTranspose2d(32, 3, kernelsize=4, stride=2, padding=1)

Table 8. Decoder for the image data.

A.8. Implementation Details

To obtain disentangled representations for the CelebA dataset, we initially employ the FastICA implementation available in the scikit-learn software on the features extracted from the pretrained ViT-B/32 encoder. Subsequently, we train the decoder, as outlined in Table 8, utilizing Mean Squared Error (MSE) loss.

In our experiments with ImageNet-Type data, we utilized the PCA and FastICA implementations provided by scikit-learn. For our proposed method, which combines PCA and ICA, we configured the number of components to 500 for PCA, and for FastICA, we set it to 160 for 1, 2, and 4-shot learning scenarios, and 200 for 8 and 16-shot learning scenarios. When employing ICA alone, we chose to use 300 components. For the proposed method with ICA only, we set number of components to 300.

Following the setting of linear probe in CLIP, we train a logistic regression classifier using scikit-learn’s L-BFGS implementation, with maximum 1,000 iterations. We determine the L2 regularization strength using a hyperparameter sweep on the validation sets over the range between 10^{-6} and 10^6 , with 96 logarithmically spaced steps. To save compute required for the sweeps, we perform a parametric binary search and iteratively halves the interval around the peak until it reaches a resolution of 8 steps per decade. The hyperparameter sweeps are performed on a validation split of each dataset.